BRNO UNIVERSITY OF TECHNOLOGY

VYSOKÉ UČENÍ TECHNICKÉ V BRNĚ

FACULTY OF MECHANICAL ENGINEERING

FAKULTA STROJNÍHO INŽENÝRSTVÍ

INSTITUTE OF MATHEMATICS

ÚSTAV MATEMATIKY

MATHEMATICAL MODEL OF MEMBRANE DISTILLATION

MATEMATICKÝ MODEL MEMBRÁNOVÉ DESTILACE

MASTER'S THESIS

DIPLOMOVÁ PRÁCE

AUTHOR — **Bc. JIŘÍ HVOŽĎA**

AUTOR PRÁCE

SUPERVISOR — **Ing. TEREZA KŮDELOVÁ, Ph.D.**

VEDOUCÍ PRÁCE

BRNO 2021

BRNO UNIVERSITY OF TECHNOLOGY
FACULTY OF MECHANICAL ENGINEERING

Assignment Master's Thesis

Institut:	Institute of Mathematics
Student:	**Bc. Jiří Hvožďa**
Degree programm:	Applied Sciences in Engineering
Branch:	Mathematical Engineering
Supervisor:	**Ing. Tereza Kůdelová, Ph.D.**
Academic year:	2020/21

As provided for by the Act No. 111/98 Coll. on higher education institutions and the BUT Study and Examination Regulations, the director of the Institute hereby assigns the following topic of Master's Thesis:

Mathematical model of membrane distillation

Brief Description:

Lack of drinking water is a very topical issue today. Therefore, various ways of obtaining it are being explored. One possibility is membrane distillation, where the mass is transferred through the porous wall. The whole process is mathematically described by differential equation. The work will deal with a new alternative of the distillation unit, which combines the use of two types of polymeric hollow fibers, namely heat and mass transfer fibers.

Master's Thesis goals:

The thesis will carry out a literature review on the topic with an emphasis on a mathematical model describing the process of membrane distillation. Next, the necessary mathematical apparatus will be examined and described on the basis of which a mathematical model will be built, which will predict the values on the output based on the entered inputs. The model will be verified with experimentally measured data.

Recommended bibliography:

BERGMAN, T. L., INCROPERA, F. P. Fundamentals of heat and mass transfer. 7th ed. Hoboken, NJ: Wiley, c2011. ISBN 978-0470-50197-9.

EVANS, L. C. Partial differential equations. 2nd ed. Providence, R.I.: American Mathematical Society, c2010. Graduate studies in mathematics, v. 19. ISBN 978-0821849743.

FARLOW, S. J. Partial differential equations for scientists and engineers. New York: Dover Publications, 1993. ISBN 978-0486676203.

BIRD, R. B., STEWART, W. E., LIGHTFOOT, E. N. Transport phenomena. 2nd, rev. ed. New York: John Wiley, c2007. ISBN 978-0470115398.

HIRSCH, M. W., SMALE, S., DEVANEY, R. L. Differential equations, dynamical systems, and an introduction to chaos. 3rd ed. Waltham, MA: Academic Press, c2013. ISBN 9780123820105.

Deadline for submission Master's Thesis is given by the Schedule of the Academic year 2020/21

In Brno,

L. S.

prof. RNDr. Josef Šlapal, CSc.
Director of the Institute

doc. Ing. Jaroslav Katolický, Ph.D.
FME dean

Abstract
The master's thesis deals with membrane distillation, particularly from the mathematical point of view. Membrane distillation is a thermally driven separation process using a porous membrane to set liquid and gas phases apart. The liquid evaporates and its vapour crosses the membrane's pores. In this process both heat and mass transfers occur. They are governed by a system of partial differential equations. Another model is built based on the analogy to electrical circuits, the first law of thermodynamics, the mass balance, and empiric relations. It is verified with experimentally measured data from a new alternative distillation unit, in which polymeric hollow fibers are used for both membrane module and condenser. The performance and efficiency of the system are evaluated, and further improvements are proposed.

Abstrakt
Diplomová práce se zabývá membránovou destilací, především z matematické perspektivy. Jedná se o tepelně poháněný separační proces, ve kterém se pro rozdělení kapalné a plynné fáze používá porézní membrána. Kapalina se vypařuje a její plynná fáze prochází přes póry v membráně. Během tohoto procesu dochází k tepelné i látkové výměně, které jsou popsány systémem parciálních diferenciálnich rovnic. Další model je založen na analogii s elektrickými obvody, zákonu zachování energie, hmotnostní bilanci a empirických vztazích. Je ověřen s experimentálně naměřenými daty z nové alternativní destilační jednotky používající membránu a kondenzátor z polymerních dutých vláken. Výkon a účinnost jednotky jsou vyhodnoceny. Další možná vylepšení jsou navržena.

Keywords
membrane distillation, desalination, polymeric hollow fibers, heat exchange, mass transfer, partial differential equations, moist air

Klíčová slova
membránová destilace, odsolování, polymerní dutá vlákna, tepelná výměna, látkový přenos, parciální diferenciální rovnice, vlhký vzduch

HVOŽĎA, Jiří. *Mathematical model of membrane distillation.* Brno, 2021. Available also at: https://www.vutbr.cz/studenti/zav-prace/detail/132088. Master's Thesis. Brno University of Technology, Faculty of Mechanical Engineering, Institute of Mathematics. Supervisor Tereza Kůdelová.

Declaration

I declare that I have written my master's thesis on the theme of 'Mathematical model of membrane distillation' independently, under the guidance of the master's thesis supervisor and using the technical literature and other sources of information which are all quoted in the thesis and detailed in the list of literature at the end of the thesis. As the author of the master's thesis I furthermore declare that, as regards the creation of this master's thesis, I have not infringed any copyright. In particular, I have not unlawfully encroached on anyone's personal and orr ownership rights, and I am fully aware of the consequences in the case of breaking Regulation § 11 and the following of the Copyright Act No 121/2000 Sb., and of the rights related to intellectual property right and changes in some Acts (Intellectual Property Act) and formulated in later regulations, inclusive of the possible consequences resulting from the provisions of Criminal Act No 40/2009 Sb., Section 2, Head VI, Part 4.

Brno 20. 5. 2021 Jiří Hvožďa

Acknowledgement

I would like to thank Ing. Tereza Kůdelová, Ph.D. for supervising my master's thesis, for all her support, advice, valuable comments, and suggestions. I would also like to express my gratitude to Heat Transfer and Fluid Flow Laboratory for allowing me to cooperate on such an innovative project.

Dále bych rád ve svém rodném jazyce poděkoval svému dobrému příteli a kolegovi „spojovník, nebo pomlčka“ Robino, právě jsi prohrál. Veliké díky patří mé rodině za nesmírnou podporu nejen při studiu, ale i během celého mého života. Děkuju moc Vlastičko a Adame. A jak se hezky česky říká, last but not least, bych chtěl poděkovat Tobě, Miška, za obrovskou podporu a trpělivost během posledních měsíců, „puky puky“.

Jiří Hvožďa

Contents

Introduction

In 2017, 71 % of the global population (5.3 billion people) used a safely managed drinking-water service, one located on-premises, available when needed, and free from contamination. It means that on Earth there were 2.2 billion people without safety managed services [1]. The oceans represent the earth's major water reservoir. About 97 % of the earth's water is sea water, while another 2 % is locked in icecaps and glaciers. Available fresh water accounts for less than 0.5 % of the earth's total water supply [2]. Moreover, conventional energy sources and fresh water reservoirs are quickly becoming in short supply. Therefore, new less energy-intensive, and more environment-friendly water purification techniques are emerging [3].

Membrane distillation (MD) is one of the recent promising separation processes. In recent years it has gained popularity due to some unique benefits. MD is a thermally driven process across a porous hydrophobic membrane (figure 1). It possesses the potential to concentrate the solutions to their saturation point without any significant permeate flux decline. Furthermore, the process can be powered by waste heat such as solar energy, geothermal energy, and waste grade energy associated with low-temperature industrial streams. MD process allows only vapour to pass. Hence the obtained product is theoretically 100 % pure from solid and nonvolatile contaminants [3].

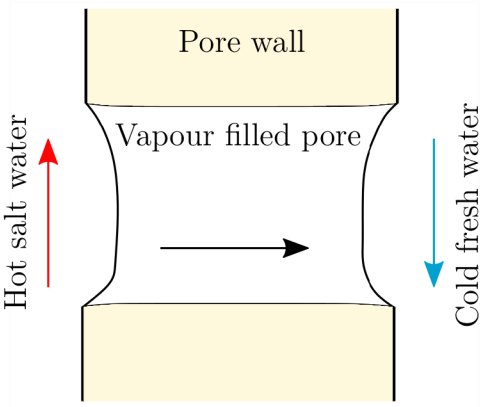

Figure 1: Principle of desalination using hydrophobic membrane [4].

In the MD process both heat and mass transfer occur. In general, they are governed by a boundary-value problem for the system of partial differential equations, which is rather difficult to solve. The most suitable approach is time-demanding simulations, which are difficult to carry because of the complexity of the membrane geometry in our particular case. Nevertheless, the important theory is carried out, and further references are provided. A less robust one-dimensional mathematical model is developed using the analogy to electrical circuits, empiric relations, and the balance of mass and energy. Heat transfer through the membrane is modelled by conduction and latent heat. Mass transfer is described by the dusty gas model combining ordinary diffusion, Knudsen diffusion, and Poiseuille flow.

The desalination process requires high corrosion resistance due to very aggressive salt water. Polypropylene, a known corrosion inhibitor, was used in the form of hollow fibers to develop a fully polymeric distillation unit in Heat Transfer and Fluid Flow Laboratory [5]. The mathematical model is verified with measured data on this unit for the varying temperatures at the membrane's input. Thermal performances and effectiveness of membrane and condenser are evaluated and compared with other previous results in referred journals.

1 Mathematical Background

The membrane distillation process is generally governed by a complicated system of partial differential equations (we shall use abbreviation PDE and PDEs for single equation and multiple equations sequentially). We introduce them via particular vectors, so-called multiindices. Necessary definitions and notation are mentioned. Last but not least, the divergence theorem is stated.

1.1 Partial Differential Equations

Most physical phenomena, whether in the domain of fluid dynamics, electricity, magnetism, mechanics, optics, or heat flow, can be described in general by PDEs. In fact, most of the mathematical physics are PDEs. Simplifications can indeed be made that reduce the equations in question to ordinary differential equations. Nevertheless, the complete description of these systems resides in the general area of PDEs [6].

Roughly speaking, a PDE is an equation involving an unknown function of two or more variables and certain of its partial derivatives [7]. To be more precise, denote Ω an open subset of $\mathbb{R}^n$, where n is a positive integer, $\mathbf{x} = (x_1, x_2, \ldots, x_n)$ be a vector of variables, and u represents a function, $u : \Omega \to \mathbb{R}$. To introduce a PDE in a general way, we use multiindex $\boldsymbol{\alpha} = (\alpha_1, \ldots \alpha_n)$, where α_i is a nonnegative integer for all $i = 1, \ldots, n$. The sum of all its elements

$$|\boldsymbol{\alpha}| = \sum_{i=1}^{n} \alpha_i$$

is called the order of the multiindex $\boldsymbol{\alpha}$ [7]. Using this multiindex, we introduce a partial differential of a function $u(\mathbf{x})$ as

$$\mathrm{D}^{\boldsymbol{\alpha}} u(\mathbf{x}) = \frac{\partial^{|\boldsymbol{\alpha}|} u(\mathbf{x})}{\partial x_1^{\alpha_1} \ldots \partial x_n^{\alpha_n}}.$$

For clarity we provide one small example, set $n = 2$, $\boldsymbol{\alpha} = (2, 1)$, then we get

$$\mathrm{D}^{(2,1)} u(\mathbf{x}) = \frac{\partial^3 u(\mathbf{x})}{\partial x_1^2 \partial x_2}, \tag{1.1}$$

we might also use different notations of equation (1.1), which follow

$$\partial x_1^2 \partial x_2 u(\mathbf{x}) = u_{x_1 x_1 x_2}(\mathbf{x}).$$

We usually omit the argument of function u and write shortly

$$\mathrm{D}^{(2,1)} u = \frac{\partial^3 u}{\partial x_1^2 \partial x_2} = \partial x_1^2 \partial x_2 u = u_{x_1 x_1 x_2}.$$

We denote the set of all partial derivatives of order $k \in \mathbb{N}$ as [8]

$$\mathrm{D}^k u(\mathbf{x}) = \left\{ \mathrm{D}^{\boldsymbol{\alpha}} u(\mathbf{x}),\ |\boldsymbol{\alpha}| = k \right\}.$$

Using the notation of multiindices, we can elegantly write the general form of a PDE of order k as

$$F\left(\mathrm{D}^k u(\mathbf{x}), \mathrm{D}^{k-1} u(\mathbf{x}), \ldots, \mathrm{D} u(\mathbf{x}), u(\mathbf{x}), \mathbf{x} \right) = 0,$$

where

$$F : \mathbb{R}^{n^k} \times \mathbb{R}^{n^{k-1}} \cdots \times \mathbb{R}^n \times \mathbb{R} \times \Omega \to \mathbb{R}$$

is given and

$$u : \Omega \to \mathbb{R}$$

is an unknown function.

The system of PDE is, informally speaking, a selection of several PDEs with several unknown functions. Following expression

$$\mathbf{F}\left(\mathrm{D}^k\mathbf{u}(\mathbf{x}), \mathrm{D}^{k-1}\mathbf{u}(\mathbf{x}), \ldots, \mathrm{D}\mathbf{u}(\mathbf{x}), \mathbf{u}(\mathbf{x}), \mathbf{x}\right) = 0$$

is called the system of partial differential equations of order k, where

$$\mathbf{F} : \mathbb{R}^{mn^k} \times \mathbb{R}^{mn^{k-1}} \cdots \times \mathbb{R}^{mn} \times \mathbb{R}^m \times \Omega \to \mathbb{R}^m$$

is given and

$$\mathbf{u} : \Omega \to \mathbb{R}^m,\ \mathbf{u} = (u_1, \ldots, u_m)$$

is an unknown vector function.

Heat and mass transfers during MD are generally governed by the system of PDEs of second order in three-dimensional space. Sometimes the last variable x_n is denoted by t and typically means time, i.e. $t > 0$. The system with prescribed values of unknown function u at some time t_0 at all points of Ω is called the initial-value problem. When the function is time-independent, then it describes a steady-state operation.

Ω is defined as an open set. A natural question may occur about what is happening on the boundaries Γ of Ω. We can set boundary conditions there to get a boundary-value problem. We usually distinguish between several types of boundary conditions: Dirichlet, Neumann, and Robin. The shape of these conditions and interpretation in PDE of heat transfer is described in table 1.1. We can also divide Γ into several disjoint parts, prescribe different conditions on each of them and get so-called mixed boundary condition.

Table 1.1: Boundary conditions for PDE with interpretation for the heat transfer boundary-value problem, $c_0, c_1 \in \mathbb{R}$, $\hat{\mathbf{n}}(\mathbf{x})$, and $u(\mathbf{x})$ are the unit normal vector of Γ, and temperature at $\mathbf{x}$ respectively, $\dot{q}$ is heat flux, and h is the overall heat transfer coefficient.

Name	Mathematical form			Heat transfer interpretation
Dirichlet	$u(\mathbf{x})$	$= f(\mathbf{x}),$	$\forall \mathbf{x} \in \Gamma$	Known u
Neumann	$\nabla u(\mathbf{x}) \cdot \hat{\mathbf{n}}(\mathbf{x})$	$= f(\mathbf{x}),$	$\forall \mathbf{x} \in \Gamma$	Known $\dot{q}$
Robin	$c_0 u(\mathbf{x}) + c_1 \nabla u(\mathbf{x}) \cdot \hat{\mathbf{n}}(\mathbf{x})$	$= f(\mathbf{x}),$	$\forall \mathbf{x} \in \Gamma$	Known h

Another important term is linearity. A PDE is either linear or nonlinear[1]. We say that a PDE is linear if we can write it in the following manner [7]

$$\sum_{|\alpha| \leq k} a_\alpha(\mathbf{x})\, \mathrm{D}^\alpha u(\mathbf{x}) = f(\mathbf{x}).$$

Finding a solution to a problem is one of the essential goals in mathematical modelling. Unfortunately, there is no general theory concerning the solvability of all PDEs. Moreover, such a theory is implausible to exist, given the rich variety of phenomena modelled by PDE [7].

[1]Fact that there also exist other types, such as quasilinear and semilinear, is omitted.

1.2 Other Important Notation

Gradient

We denote some special symbols related to derivatives. For function u we define the gradient of u as

$$\nabla u = \left(u_{x_1}, u_{x_2}, \ldots, u_{x_n}\right).$$

Divergence

The sum of all elements of the gradient of a function u is called divergence of the function u, written as

$$\nabla \cdot u = \sum_{i=1}^{n} u_{x_i}.$$

Laplace Operator

For a function u, we define the Laplace operator as the divergence of the gradient of u. Note that it is very often denoted by Δu. However, we use $\nabla \cdot \nabla u$ notation exclusively, preventing the confusion with pressure and temperature differences to which symbol Δ is devoted.

Double Dot Operator

For two square matrices $\boldsymbol{A}$ and $\boldsymbol{B}$ with n columns and rows with elements A_{ij} and B_{ij} respectively, the double dot operator is defined as a map $\mathbb{R}^{n^2} \times \mathbb{R}^{n^2} \to \mathbb{R}$ in the following way

$$\boldsymbol{A} : \boldsymbol{B} = \sum_{i=1}^{n} \sum_{j=1}^{n} A_{ij} B_{ij}. \tag{1.2}$$

1.3 Divergence Theorem

Let's think of divergence as a derivative of sorts. Then the divergence theorem relates a volume integral of derivative $\nabla \cdot \mathbf{F}$ over a solid to a flux integral of $\mathbf{F}$ over the boundary of the solid. More specifically, the divergence theorem relates a flux integral of vector field $\mathbf{F}$ over a closed surface Γ to a volume integral of the divergence of $\mathbf{F}$ over the solid enclosed by Ω [9].

Let Ω be a simple region[2] in space, and let Γ be the surface of Ω with $\hat{\mathbf{n}}$ the outward pointing unit normal. Let $\mathbf{F}$ be a vector field defined on Ω. Then

$$\int_{\Omega} \nabla \cdot \mathbf{F} \, \mathrm{d}\mathbf{x} = \int_{\Gamma} \mathbf{F} \cdot \hat{\mathbf{n}} \, \mathrm{d}\Gamma. \tag{1.3}$$

In a word, the total flux across the boundary of Ω equals the total divergence in Ω [9].

[2] In plane, a simple region is such that it is elementary in both x and y directions. Being elementary in direction x means that the domain is bounded with two horizontal lines from above and below and by two continuous curves from left and right. A simple region in three-dimensional space is elementary in all three space directions x, y, and z. We say that a region is elementary in direction z, if there is an elementary region D in xy plane and a pair of continuous functions $\gamma_1(x, y)$ and $\gamma_2(x, y)$ defined on D, such that Ω consists of those triples (x, y, z) for which $(x, y) \in D$ and $\gamma_1(x, y) \leq z \leq \gamma_2(x, y)$.

2 Heat Transfer

Thermomechanics has two main branches. Thermodynamics dealing with changes in an isolated system. Heat transfer is introduced for the evaluation of heat rate. The subjects of both branches are complementary and interrelated. On the other hand, they have fundamental differences. Heat transfer is thermal energy in transit due to spatial temperature difference. Whenever a temperature difference occurs in a medium or between media, heat transfer must occur. There exist three modes of heat transfer [10]:

- conduction,
- convection,
- radiation.

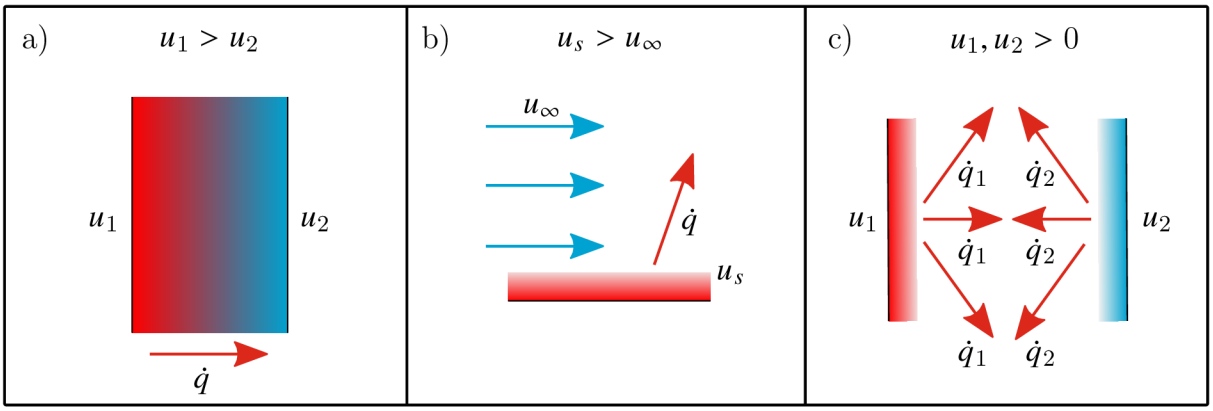

Figure 2.1: Heat transfer modes. a) conduction through solid material or nonflowing liquid, b) convection between flowing liquid and surface of solid material, c) radiation of two surfaces [10].

2.1 Radiation

All surfaces of finite temperature emit energy in the form of electromagnetic waves. Hence, there is heat transfer by radiation between two surfaces at different temperatures in the absence of an intervening medium, see figure 2.1 c). The energy of the radiation field is transported by electromagnetic waves (or photons). While the transfer of energy by conduction or convection requires the presence of a material medium, radiation does not. In fact, radiation transfer occurs most efficiently in a vacuum. Radiation can be modelled by Stefan-Boltzmann law

$$E = \sigma u_s^4,$$

where E is emissive power, $\sigma = 5.67 \cdot 10^{-8}\ \mathrm{W \cdot m^{-2} \cdot K^{-4}}$ is Stefan-Boltzmann constant and u_s is the surface temperature [10]. In the modelling of membrane distillation, transferred energy due to radiation is omitted because the effect is negligible.

2.2 Conduction

Conduction is the heat transfer that happens inside a medium due to the existing temperature gradient. The physical mechanism is one of random atomic or molecular activity. Let us provide a simple example, see figure 2.1 a). Consider gas inside a box. One of the sides is hotter than the opposite one. Thus, molecules of gas in the hotter part are having higher energy. Hence they are moving faster. As we know, molecules can collide with each other. When a collision occurs, some energy is transferred from the more energic to the less energic molecule. Conduction is governed by Fourier's law

$$\dot{\mathbf{q}} = -\lambda \nabla u, \tag{2.1}$$

where the $\dot{\mathbf{q}}$ is the vector of heat fluxes, λ is thermal conductivity, and u is temperature. We can compute heat transfer rate q as multiplication of heat flux and size of the orthonormal area, through which heat exchange is happening,

$$q = \dot{\mathbf{q}} A. \tag{2.2}$$

The minus sign in (2.1) is meaningful. It tells that the heat flux is positive in the direction of decreasing temperature. Thermal conductivity is the characteristic of a material. In general, it has different values in different directions. Materials that have the same λ in all directions are called isotropic. The thermal conductivity of solid materials is usually higher than liquids, which is higher than gases. The main reason is the difference in intermolecular distances in those states. Lower distance means a higher probability of collision, thus a higher probability of energy transfer from one molecule to another. Therefore, the physical mechanism of conduction is described mainly by $\dot{q}$. Very often, thermal conductivity is considered to be a constant for various materials [10].

2.2.1 The Heat Diffusion Equation

A primary objective in a conduction analysis is to determine how temperature varies with the position in the medium in time. Once the distribution is known, one can compute heat flux at any point of domain Ω of medium or on its surface Γ using Fourier's Law (2.1). Other significant quantities might also be determined [10]. The heat diffusion equation might be derived for stationary homogenous isotropic solid with heat generation within the body. The heat generation rate in the medium generally specified as heat generation per unit time is denoted as $q'(\mathbf{x}, t)$. Heat generation might be due nuclear, electrical, chemical, or other sources that might be a function of position and time.

The energy balance equation for a small control volume W illustrated in figure 2.2 is stated as

$$\begin{bmatrix} \text{Rate of heat entering through} \\ \text{the bounding surfaces } W \end{bmatrix} + \begin{bmatrix} \text{Rate of energy} \\ \text{generation in } W \end{bmatrix} = \begin{bmatrix} \text{Rate of storage} \\ \text{of energy in } W \end{bmatrix}. \tag{2.3}$$

We can evaluate terms in equation (2.3) as

$$\begin{bmatrix} \text{Rate of heat entering through} \\ \text{the bounding surfaces } W \end{bmatrix} = -\int_{\Gamma} \dot{\mathbf{q}} \cdot \hat{\mathbf{n}} \, \mathrm{d}\Gamma = -\int_{W} \nabla \cdot \dot{\mathbf{q}} \, \mathrm{d}\mathbf{x}, \tag{2.4}$$

where Γ is the surface area of the volume element W, $\hat{\mathbf{n}}$ is the outward-drawn normal unit vector to the surface element $\mathrm{d}\Gamma$. The minus sign is included to ensure that heat flow is

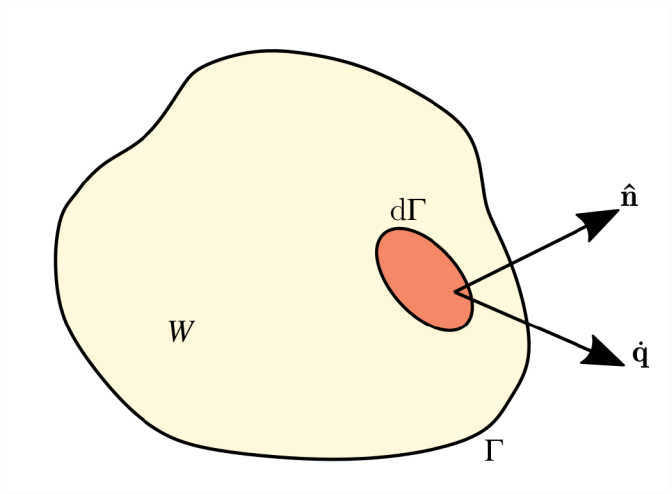

Figure 2.2: Control volume for the derivation of the heat conduction equation [11].

into the volume element. The divergence theorem (1.3) is used to convert surface integral to volume integral. Other terms follow as

$$\left[\begin{array}{c}\text{Rate of energy}\\ \text{generation in } W\end{array}\right] = \int_W q'(\mathbf{x},t)\,\mathrm{d}\mathbf{x}, \tag{2.5}$$

$$\left[\begin{array}{c}\text{Rate of storage}\\ \text{of energy in } W\end{array}\right] = \int_W \rho C_p \frac{\partial u\,(\mathbf{x},t)}{\partial t}\,\mathrm{d}\mathbf{x}. \tag{2.6}$$

C_p is the specific heat. The substitution of equations (2.4)–(2.6) into (2.3) yields

$$\int_W \left[-\nabla\cdot\dot{\mathbf{q}} + q'(\mathbf{x},t) - \rho C_p \frac{\partial u\,(\mathbf{x},t)}{\partial t}\right]\mathrm{d}\mathbf{x} = 0. \tag{2.7}$$

Equation (2.7) is derived for arbitrary small-volume element W within the solid, hence, the volume might be chosen so small that the integral is removed. We obtain

$$-\nabla\cdot\dot{\mathbf{q}} + q'(\mathbf{x},t) = \rho C_p \frac{\partial u\,(\mathbf{x},t)}{\partial t}. \tag{2.8}$$

Using Fourier's law (2.1) to express heat flux in (2.8), we obtain the differential equation of heat conduction for stationary homogenous isotropic solid with heat generation within the body as nonlinear second order PDE:

$$\nabla\cdot[\lambda\nabla u(\mathbf{x},t)] + q'(\mathbf{x},t) = \rho C_p \frac{\partial u\,(\mathbf{x},t)}{\partial t}. \tag{2.9}$$

To which initial and boundary conditions might be prescribed. For specific configurations of equation (2.9), one can solve the problem using the Fourier series method to find the analytical solution. From the numerical perspective, the difference method or finite elements method can be used [11].

2.3 Convection

Convection describes energy transfer between a surface and fluid moving over the surface. It includes energy transfer by both the bulk fluid motion (advection) and the random

motion of fluid molecules (conduction or diffusion). Newton's cooling governs heat flux in the normal direction to the surface as

$$\dot{q}_n = \dot{\mathbf{q}} \cdot \hat{\mathbf{n}} = h^*(u_s - u_\infty), \tag{2.10}$$

where h^* is the convective heat transfer coefficient, u_s is the temperature at the surface, and u_∞ is the temperature of the free stream [10].

2.3.1 Boundary Layers

For convection analysis, there are several important facts connected with hydrodynamics. Let us start with the notion of boundary layers. Suppose we have a plane desk to which a stream is approaching with velocity v_∞ and temperature u_∞, see figure 2.3. Subscript ∞ refers to properties of the free stream. Moreover, assume that the surface of the desk has a constant temperature $u_s > u_\infty$. Due to viscosity[1] the velocity of the stream closer to the surface of the desk is magnificently decreasing. In such a manner that at the surface, the fluid velocity is equal to zero. We define the velocity boundary layer at point x as interval $(0, \delta_v(x))$, where $\delta_v(x) \in \mathbb{R}^+$ is the width of the velocity boundary layer at point x determined from

$$v(x, \delta_v(x)) = 0.99 v_\infty \text{ and } \delta_v(x) = \min_{y \in \mathbb{R}^+} \{v(x, y) \geq 0.99 v_\infty\}.$$

Analogously, the thermal boundary layer at point x is defined as the interval $(0, \delta_u(x))$, where $\delta_u(x) \in \mathbb{R}^+$ is the width of the thermal boundary layer at point x evaluated from

$$u_s - u(x, \delta_u(x)) = 0.99(u_s - u_\infty) \text{ and } \delta_u(x) = \min_{y \in \mathbb{R}^+} \{(u_s - u(x, y)) \geq 0.99(u_s - u_\infty)\}.$$

For arbitrary $x > 0$ and $y = 0$ we got from Fourier's Law (2.1)

$$\dot{q} = -\lambda \frac{\partial u}{\partial y}\Big|_{y=0}. \tag{2.11}$$

Combine (2.11) with Newton's cooling law (2.10) and express convective heat transfer, we get

$$h^* = \frac{-\lambda}{(u_s - u_\infty)} \frac{\partial u}{\partial y}\Big|_{y=0}. \tag{2.12}$$

Unlike thermal conductivity, heat transfer coefficient cannot be taken as a material constant, as we can see in (2.12), convective heat transfer coefficient is strongly depending on partial derivative of temperature by y. In our simple example in figure 2.3 for increasing x, the partial derivative of temperature with respect to y is decreasing. Hence, the heat transfer coefficient is also decreasing for x increasing. From this argument, one can realize that determining h^* is a rather complicated task.

For flow over any surface, there always exist both hydrodynamic and thermal boundary layers. Hence, the surface friction exists without exception. Thus, convection heat transfer occurs if temperatures of the surface and free stream differ.

The temperature gradient at the surface in previous equations can be interpreted as the dimensionless parameter called Nusselt number (denoted by Nu). It is a ratio of convection to pure conduction heat transfer across the boundary [10].

[1] Viscosity is a measure of a fluid's resistance to flow. It describes the internal friction of moving fluid.

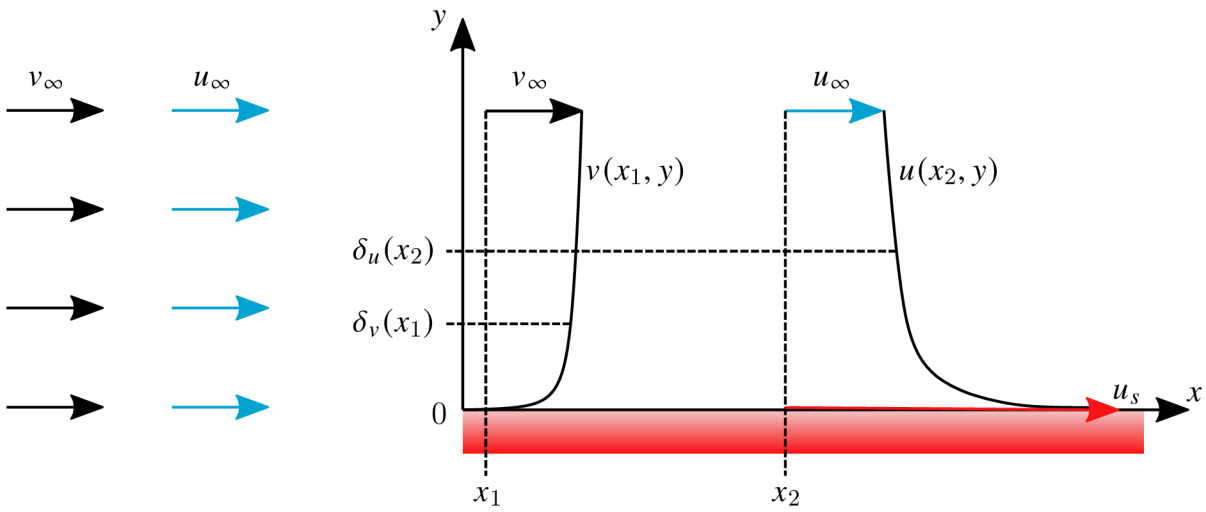

Figure 2.3: Hydrodynamic boundary layer at point x_1 and thermal boundary layer at point x_2 [10], [12].

2.3.2 Flow Conditions

In the discussion of convection so far, we have not addressed the significance of the flow conditions. An essential step in treating any convection problem is determining whether the boundary layer is laminar or turbulent. Surface friction and the convection transfer rates depend strongly on which of these conditions exist [10]. In the laminar boundary layer, the fluid flow is highly ordered and it is possible to identify streamlines[2] along which fluid particles move. Flow in the fully turbulent boundary layer is generally highly irregular and is characterized by a random, three-dimensional motion of relatively large parcels of fluid. Mixing within the boundary layer carries high-speed fluid toward the solid surface and transfers slower-moving fluid farther into the free stream (see figure 2.4). Much of the mixing is promoted by streamwise vortices called streaks generated intermittently near the flat plate, where they rapidly grow and decay. Recent analytical and experimental studies have suggested that these and other coherent structures within the turbulent flow can travel in waves at velocities that can exceed v_∞, interact nonlinearly, and spawn the chaotic conditions that characterize turbulent flow [13].

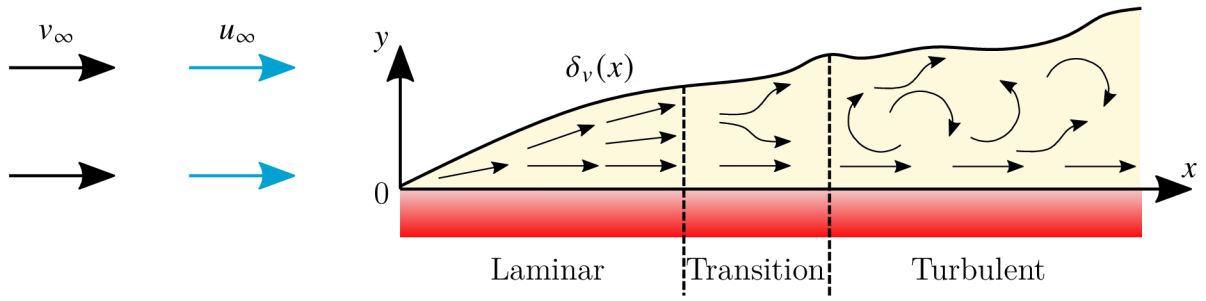

Figure 2.4: Hydrodynamic boundary layer for different modes of flow along a plane desk [10].

There exists a transition zone between those two modes. In which the boundary layer is neither laminar nor turbulent, conditions within the transition zone change with time. The flow sometimes exhibits laminar behaviour and sometimes shows the characteristics of turbulent flow.

[2]Streamline is the path traced by a particle in fluid moving in smooth flow without turbulence.

To decide whether the flow is in laminar mode, dimensionless Reynolds number defined as

$$\mathrm{Re} = \frac{\rho v_\infty L}{\mu},$$

is often used. The density of the medium is represented by ρ, L is the characteristic length, and μ is the dynamic viscosity. For given problems, there exists a critical Reynolds number Re_c. If $\mathrm{Re} > \mathrm{Re}_c$ then transition from laminar flow occurs.

2.3.3 Latent Heat

The process of membrane distillation is associated with the fluid phase change. In particular, solid-liquid and solid-vapour interfaces occur, namely boiling and condensation. They are classified as forms of convection mode of heat transfer, although unique features characterize them. Latent heat effects associated with the phase change are significant. Since it is difficult to develop governing equations for boiling and condensation processes, we provide an equation for the heat flux in the membrane due to evaporation as

$$\dot{q}_v = j\Delta H_v, \tag{2.13}$$

where j is the permeate flux[3] through the membrane and ΔH_v is the latent heat of evaporation. Assuming that all the generated vapour is condensed at the condenser in a closed system, equation (2.13) also holds for heat flux due to the condensation (only with minus sign on the right side) [10], [14].

2.4 The Overall Heat Transfer Coefficient

One of the most important parameters of heat exchangers is the overall heat transfer coefficient h (we use abbreviation HTC) with dimension $\mathrm{W{\cdot}m^{-2}{\cdot}K^{-1}}$. It tells us how much heat is transferred through the area with the size of one square meter if temperatures difference Δu between hot and cold fluid is one kelvin [15]. Overall heat flux of a heat exchanger might be expressed as [10]

$$\dot{q} = h\Delta u. \tag{2.14}$$

2.4.1 Thermal Resistance Approach

HTC strongly depends on the geometry of the heat exchanger, the thermal conductivity of used materials, and convective heat transfer coefficient. The usual approach is to evaluate the overall thermal resistance R_u of the system, and HTC is its inverse. This approach is derived from the differential equation of heat conduction (2.9) with assumptions: steady-state operation, no energy is generated inside the volume element, and the temperature functions depend only on x direction.

For illustration, consider the example illustrated in figure 2.5 with two walls having different thicknesses δ_1, δ_2 and conductivities λ_1, λ_2. We identify the total thermal

[3]Permeate flux describes the permeate quantity produced during MD per unit of time and membrane area.

resistance as composition[4] of four (two conduction and two boundary layer) resistances in series. Overall thermal resistance follows as

$$R_t = \frac{\delta_1}{\lambda_1} + \frac{\delta_2}{\lambda_2} + \frac{1}{h_1^*} + \frac{1}{h_2^*}.$$

Thus,

$$h = \frac{1}{R_u}.$$

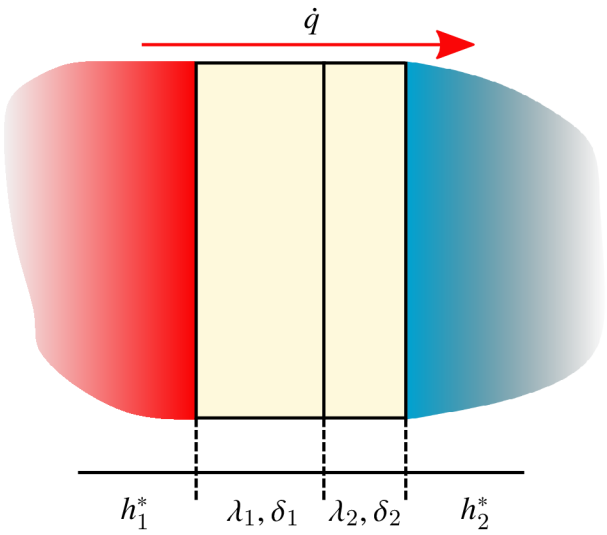

Figure 2.5: Two adjacent walls surrounded by hot liquid from the left and cold liquid from the right side. Thermal resistances in series, boundary layer resistance with convective transfer coefficient h_1^*, conduction resistance through two walls with different thicknesses and thermal conductivities, and boundary layer resistance with convective transfer coefficient h_2^*.

Equations (2.11) and (2.12) show that evaluating the convective heat transfer coefficient is a rather complicated task. Hence, also evaluating overall thermal resistance can be difficult. Equation (2.14) can be used the other way around. From known heat flux and temperature difference, we get HTC. We use the definition of heat rate (2.2) to replace heat flux in (2.14) and express HTC as

$$h = \frac{q}{A\Delta u}. \tag{2.15}$$

Consider the hollow cylindrical wall of length L with inner radius r_0 and outer radius r_1, with liquids inside and outside the cylinder with different temperatures. The wall has thermal conductivity λ_1; h_1^* and h_2^* are heat transfer coefficients inside and outside the cylinder, respectively. Then the total thermal resistance is given as

$$R_u = \frac{1}{h_1^* 2\pi r_0 L} + \frac{\ln\left(r_0 r_1^{-1}\right)}{\lambda_1 2\pi L} + \frac{1}{h_2^* 2\pi r_1 L}.$$

[4]Composition of resistors in the sense of electrical circuits. The overall resistance of resistors in series is the sum of the individual resistance values. The inverse of the overall resistance of resistors in parallel is the sum of the inverses of individual resistance values.

2.4.2 Logarithmic Mean Temperature Difference

Heat transfer rate can be computed from the first law of thermodynamics. It is pleasant to have constant HTC for given systems and conditions to compare them easily and predict heat exchange performance. To do so, we can use the logarithmic mean temperature difference method, whereas Δu is replaced in equation (2.15) by constant mean temperature difference Δu_{lm}.

In the following, subscripts h and c denote hot and cold channels of the heat exchanger, i and o hold for input and output of the channel of a heat exchanger, i is the specific enthalpy, and $\dot{m}$ is the mass flow rate. Consider a heat exchanger with the parallel arrangement, see figure 2.6. Suppose a steady-state thermal isolated system with no generated energy, a small change of kinetic and potential energies, constant heat flux. The first law of thermodynamics on a small element of the heat exchanger holds. Thus, for hot and cold channels following equality is satisfied

$$\mathrm{d}q = -\dot{m}_h \,\mathrm{d}i_h = \dot{m}_c \,\mathrm{d}i_c. \tag{2.16}$$

Moreover, suppose that media are not changing phases, specific heat capacity is constant. Thus, we can express enthalpy using specific heat and temperature, expression (2.16) is transformed into

$$\mathrm{d}q = -\dot{m}_h c_h \,\mathrm{d}u_h = \dot{m}_c c_c \,\mathrm{d}u_c.$$

Equation (2.15) yields

$$\mathrm{d}q = h\Delta u \,\mathrm{d}A. \tag{2.17}$$

Set $\Delta u = u_h - u_c$, it is a continuous function depending on the position. Hence, expression $\mathrm{d}(\Delta u)$ is meaningful. For the change of temperature difference yields

$$\mathrm{d}(\Delta u) = \mathrm{d}(\Delta u_h) - \mathrm{d}(\Delta u_c) = -\frac{\mathrm{d}q}{\dot{m}_h c_h} - \frac{\mathrm{d}q}{\dot{m}_c c_c} = -\,\mathrm{d}q \left(\frac{1}{\dot{m}_c c_c} + \frac{1}{\dot{m}_h c_h}\right). \tag{2.18}$$

In (2.18) express $\mathrm{d}q$ from (2.17)

$$\mathrm{d}(\Delta u) = -h\Delta u \left(\frac{1}{\dot{m}_c c_c} + \frac{1}{\dot{m}_h c_h}\right) \mathrm{d}A. \tag{2.19}$$

Divide both sides of (2.19) by Δu and integrate the equation, the meaning of the integral bounds is explained in figure 2.6 a),

$$\int_{\Delta u_1}^{\Delta u_2} \frac{1}{\Delta u}\,\mathrm{d}(\Delta u) = -\int_A h \left(\frac{1}{\dot{m}_c c_c} + \frac{1}{\dot{m}_h c_h}\right) \mathrm{d}A = -Ah \left(\frac{1}{\dot{m}_c c_c} + \frac{1}{\dot{m}_h c_h}\right).$$

We integrate the left side as $\ln(\Delta u)$, and we get the equation

$$\ln\frac{\Delta u_2}{\Delta u_1} = -Ah \left(\frac{1}{\dot{m}_c c_c} + \frac{1}{\dot{m}_h c_h}\right) = -Ah \left(\frac{u_{c,o} - u_{c,i}}{q} + \frac{u_{h,i} - u_{h,o}}{q}\right). \tag{2.20}$$

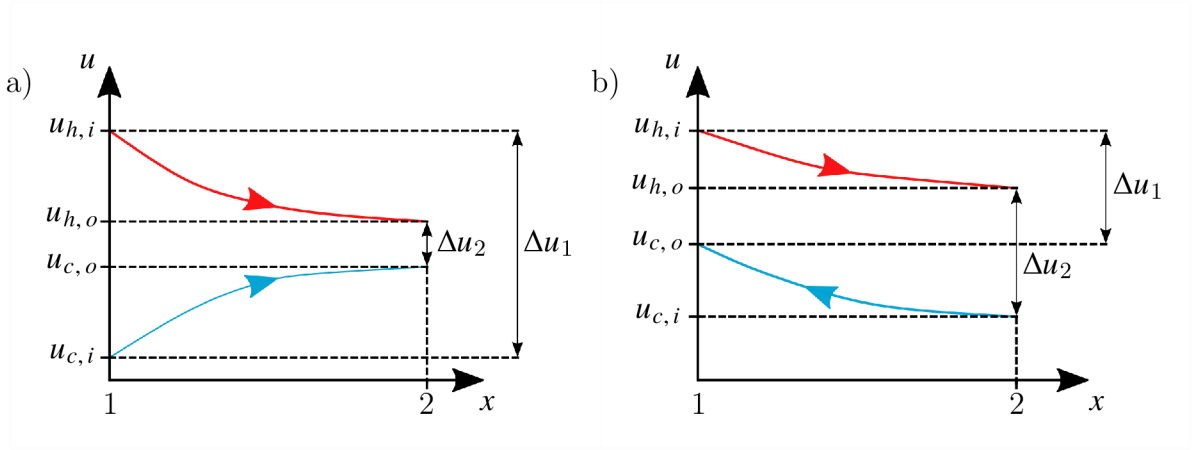

Figure 2.6: Change of temperature in a heat exchanger, a) parallel and b) counter arrangement. '1' denotes the left and '2' the right ends of a heat exchanger [10].

Multiply both sides of (2.20) by q, divide by left side of (2.20) and multiply parentheses on the right side by -1. Then we get the heat transfer rate

$$q = Ah\frac{(u_{h,o} - u_{c,o}) - (u_{h,i} - u_{c,i})}{\ln\dfrac{\Delta u_2}{\Delta u_1}} = Ah\frac{\Delta u_2 - \Delta u_1}{\ln\dfrac{\Delta u_2}{\Delta u_1}} = Ah\Delta u_{\mathrm{lm}}.$$

We see that to determine HTC, we have to know heat transfer surface area A, we have to measure differences of temperatures at input Δu_1 and output Δu_2, the heat transfer rate may be calculated from the first law of thermodynamics. Analogously, we can get the same result for counterflow arrangement, but Δu_1 and Δu_2 are defined as

$$\Delta u_1 = u_{h,i} - u_{c,o} \text{ and } \Delta u_2 = u_{h,o} - u_{c,i}.$$

Arrangements differences are demonstrated in figure 2.6. In the case of heat exchanger in crossflow arrangement, logarithmic mean temperature difference $\Delta u_{\mathrm{m,C}}$ is computed from the counterflow arrangement's logarithmic mean temperature difference $\Delta u_{\mathrm{m,CF}}$ as

$$\Delta u_{m,\mathrm{C}} = F\Delta u_{m,\mathrm{CF}}, \tag{2.21}$$

where correction factor F is computed from N, so-called number of transfer units of the measured heat exchanger and N_{CF} number of transfer units of the same exchanger but with counterflow arrangement as [10], [16]

$$F = \frac{N_{\mathrm{CF}}}{N}.$$

2.5 Effectiveness of Heat Exchangers

Theoretical transferred heat through a heat exchanger is maximized when the arrangement is counterflow

$$q_{\max} = \min\left\{\dot{m}_h c_h, \dot{m}_c c_c\right\}\left(u_{h,i} - u_{c,i}\right) = C_{\min}\left(u_{h,i} - u_{c,i}\right),$$

$C_{\min}$ is the minimal thermal capacitance of either hot or cold media in the system. It is typical to define effectiveness[5] η_{he} as the fraction of the actual and the theoretical maximal transferred heats

$$\eta_{\text{he}} = \frac{q}{q_{\max}} \cdot 100\ \%.$$

The number of transfer units N is a dimensionless parameter that is widely used for heat exchanger effectiveness analysis and is defined as

$$N = \frac{hA}{C_{\min}}, \tag{2.22}$$

In the same manner, we also define $C_{\max}$. The hot condensing medium on the condenser is using energy on change of phase and not on changing temperature. Thus, from the definition[6] of thermal capacitance $C_{\max} = C_h \to \infty$. Obviously $C_{\min} = \dot{m}_c c_{c,p}$. Relations between N and effectiveness for condenser follow

$$\eta_{\text{he}} = 1 - \exp(-N),$$
$$N = -\ln(1 - \eta_{\text{he}}).$$

In the case of heat exchangers and this type of effectiveness, it is not true that $\eta_H \to 1$ is the desired case because it forces $N \to \infty$. From the definition (2.22) it means, that either $hA \to \infty$ or $C_{\min} \to 0$. In other words, the area of the heat exchanger is too large, or its capacity is not used effectively [10], [15].

2.6 Particular Application of Nusselt Number

For evaluating the convective heat transfer coefficient of the membrane module in the experiment, we use the approach proposed by Hickman [17]. The membrane module can be interpreted as the polymeric hollow fiber heat exchanger in the crossflow configuration. Hot water flows inside the fibers and moist air crosses the heat exchanger. Suppose that the tube-side flow is fully developed laminar. The overall heat transfer coefficient is determined from computed heat flux. Tube-side and air-side heat transfer coefficients have to be evaluated to calculate temperatures on the heat exchanger surface. The overall Nusselt number is computed as

$$\text{Nu}_o = \frac{hd_i}{\lambda_w}, \tag{2.23}$$

where h is the known overall heat transfer coefficient of the heat exchanger. Fibers have the inner and outer diameter d_i and d_o sequentially. The thermal conductivity of water is λ_w. The positive root of the quadratic polynomial

$$\left(1 - \frac{59}{220}\text{Nu}_o\right)\text{Nu}_m^2 + \left(\frac{48}{11} - 2\text{Nu}_o\right)\text{Nu}_m - \frac{48}{11}\text{Nu}_o \tag{2.24}$$

[5] We stress that we talk about the effectiveness of a heat exchanger with the subscript 'he' because we also define the effectiveness of membrane in later sections.

[6] Thermal capacitance is the amount of heat that has to be supplied to the given mass to induce the change of temperature by one kelvin.

is the membrane wall Nusselt number. Finally, the Nusselt number under the Robin boundary condition is obtained as

$$\mathrm{Nu}_r = \frac{\frac{48}{11} + \mathrm{Nu}_m}{1 + \frac{59}{220}\mathrm{Nu}_m}. \tag{2.25}$$

The tube-side and air-side heat transfer coefficient are determined as

$$h_f^* = \frac{\mathrm{Nu}_r \lambda_w}{d_i} \tag{2.26}$$

and

$$h_a^* = \frac{d_o}{d_i} \cdot \frac{2\lambda_m h_f^* h}{2\lambda_m \left(h_f^* - h\right) - d_i h_f^* h} \tag{2.27}$$

respectively, λ_m is the thermal conductivity of the membrane module.

3 Mass Transport

We have learned that heat is transferred if there is a temperature difference in a medium. Similarly, if there is a difference in the concentration of some chemical species[1] in a mixture, the mass transfer must occur. Mass transfer is mass in transit as the result of a species concentration difference in a mixture [10]. We focus on three mechanisms, ordinary diffusion, Knudsen diffusion, and Poiseuille (viscous) flow, which control MD [14].

Mass transport can be modelled by overall mass resistance R_m, similarly as in section 2.4.1, where heat transfer is modelled via overall thermal resistance. Permeate flux generated by the membrane is defined as

$$j_v = \frac{\Delta p}{R_m}, \tag{3.1}$$

where Δp is the water vapour pressure difference between the membrane sides. Mass transfer resistances are illustrated in figure 3.1. In a thermally driven MD process, the increase of the overall resistance to mass transfer due to the presence of a mass transfer boundary layer in the proximity of the membrane interface is generally negligible [19]. Also, surface diffusion is considered negligible in MD modelling [20]. Three other mechanisms are connected using a dusty-gas-model (DGM) describing mass transport in the porous media [21].

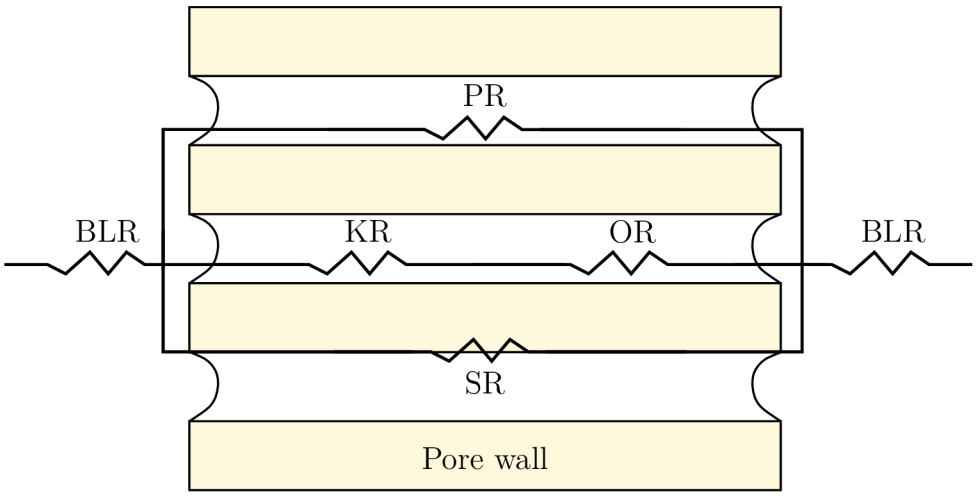

Figure 3.1: Arrangement of resistances to mass transport in MD. BLR - boundary layer resistance, KR - Knudsen resistance, OR - ordinary resistance, PR - Poiseuille resistance, SR - surface resistance [14], [22]

To decide which of three mechanisms (two or three can arise simultaneously) occur in MD, we use Knudsen number K defined as the ratio of the mean free path ℓ of transported molecules to the membrane pore size (taken as its mean value) $\overline{r}$ [23]. The average distance travelled by molecules to make collisions is defined as

$$\ell = \frac{k_B u}{\sqrt{2}\pi \overline{p} d_e^2},$$

[1] Term chemical entities stands for any constitutionally or isotopically distinct atom, molecule, ion, ion pair, radical, radical ion, complex, conformer, etc. identifiable as a separately distinguishable entity. An ensemble of chemically identical molecular entities that can explore the same set of molecular energy levels on the time scale of the experiment is called chemical species. The term is applied equally to a set of chemically identical atomic or molecular structural units in a solid array [18].

where k is Boltzmann constant, u is absolute temperature, $\overline{p}$ is average pressure within membrane pores, and d_e is the diameter of gas molecules[2] [14]. The mean free path of water vapour molecules was estimated to be 0.11 μm at 60 °C [24].

3.1 Ordinary Diffusion

For the ordinary diffusive mass flux $\mathbf{j}_A$ of species A to species B in a binary gas mixture[3] in figure 3.2, Fick's law holds

$$\mathbf{j}_A = -\rho D_{AB} \nabla m_A.$$

The mass diffusivity is represented by D_{AB} and m_A is the amount of species A in the mixture called mass fraction,

$$m_A = \frac{\rho_A}{\rho} = \frac{\rho_A}{\rho_A + \rho_B} \text{ and } \rho_i = M_i y_i, \text{ for } i = A, B,$$

where ρ_i, M_i, and y_i are density, molecular weight, and molar concentration of species i respectively. As ordinary diffusion, we understand the thermal motion of molecules at temperatures above absolute zero. The rate of this movement is a function of temperature, fluid viscosity, size, and the shape of the particles. It models intermolecular diffusion [25].

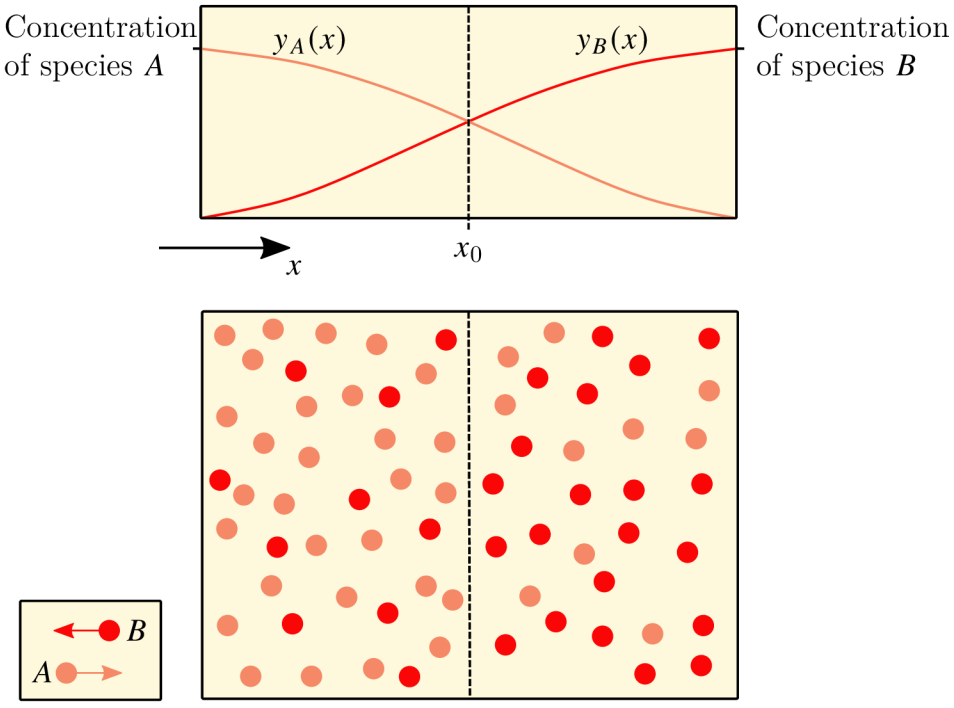

Figure 3.2: Mass transfer by the ordinary diffusion in a binary gas mixture [10].

[2] It is an idealization from the kinetic theory of gases, whereas the molecules are assumed to be hard spheres.

[3] Consider a chamber where two different gas species at the same temperature and pressure are initially separated by a partition at x_0. If the partition is removed without disturbing the fluid, both species will be transported by diffusion. Figure 3.2 shows the situation as it might exist shortly after the removal of the partition. A higher concentration means more molecules per unit volume, and the concentration of species A (light dots) decreases with increasing x, while the concentration of B increases with x [10].

For the modelling of ordinary diffusion of multicomponent mixture with N components, the Maxwell-Stefan equations

$$\nabla Y_A = -\sum_{B=1}^{N} \frac{1}{yD_{AB}} \left(Y_A \mathbf{N}_A - Y_B \mathbf{N}_B\right) \text{ for } A = 1, \ldots N$$

can be used, Y_i, y, and $\mathbf{N}_i$ are a molar fraction of component i, the overall molar concentration, the cumulative molar flux of component i respectively. The Stefan–Maxwell model is also reported to be more accurate than Fick's law for separation of azeotropic[4] mixtures [25], [27].

3.2 Knudsen Diffusion

Knudsen diffusion is a result of collisions of gas molecules with the pore walls rather than intermolecular collisions [28]. Intuitively, it occurs when the gas density is low, or the pore size is so small that collisions between molecules can be ignored compared to collisions of molecules with the inside walls of the porous membrane [29]. We illustrate the differences between ordinary and Knudsen diffusions in figure 3.3.

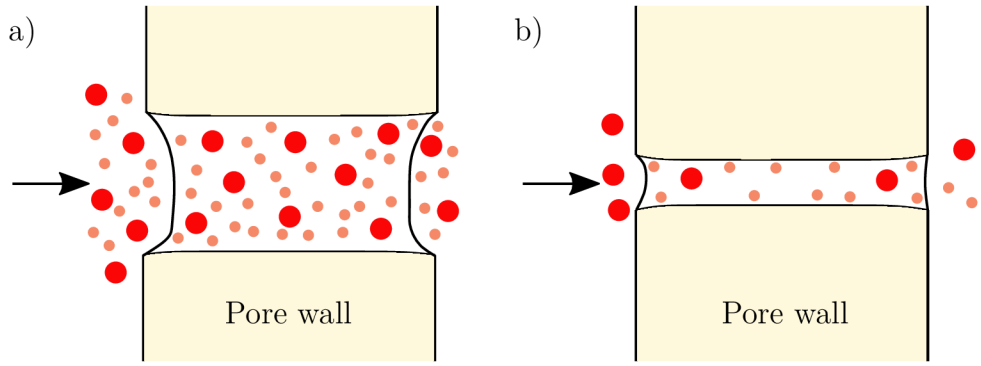

Figure 3.3: Comparison of diffusions. a) ordinary diffusion - collisions happen mainly intermolecularly, b) Knudsen diffusion - collisions happen mainly with pore walls (yellow colour) [30].

3.3 Poiseuille Flow

In Poiseuille flow, also called viscous flow, the gas molecules act as a continuous fluid driven by a pressure gradient [14]. It is a particular case of the Navier-Stokes equation for pressure-induced steady-state fluid flow in infinitely long, translation-invariant channels [31]. In this case, molecule-molecule collisions dominate over molecule-wall collisions. The influence of the Poiseuille flow can be neglected when the pore size of the membrane is relatively small (when the diameter is less than 0.1 μm) [29].

[4]The term azeotrope means 'nonboiling by any means' and denotes a mixture of two or more components where the equilibrium vapour and liquid compositions are equal at a given pressure and temperature. More specifically, the vapour has the same composition as the liquid, and the mixture boils at a temperature other than that of the pure components' boiling points [26]. Therefore, azeotropic solutions cannot be separated by conventional distillation. Membrane distillation is one of the techniques proposed to overcome this issue with an azeotrope [27].

4 Membrane Distillation

Membrane distillation is a distillation process in which the liquid and gas phases are separated by a porous membrane, the pores are not wetted by the liquid phase. It is a thermally driven separation process whereby vapour molecules are transferred or distilled through a microporous nonwetted hydrophobic membrane, see figure 4.1. The driving force is the vapour pressure difference induced by the temperature difference between the two sides of the membrane pores. Thus, simultaneous mass and heat transfer occur [14].

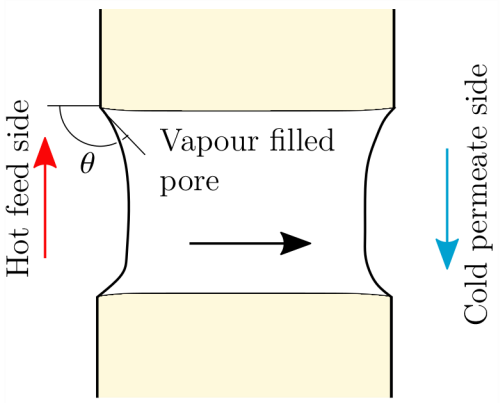

Figure 4.1: Membrane distillation principle and contact angle θ [4].

Membrane distillation operates at a lower temperature than ordinary distillation, as well as at lower hydrostatic pressures than in other membrane-based processes [32]. Therefore, MD is expected to be a cost-effective process, requiring less demanding membrane characteristics [14].

On the other hand, MD is also attended by some drawbacks such as low permeate flux (compared to other separation processes), high susceptibility permeate flux to the concentration and temperature of the feed conditions due to the concentration and temperature polarization phenomenon. Also, the trapped air within the membrane introduces a further mass transfer resistance, limiting the MD permeate flux. Moreover, the heat lost by conduction is relatively large [14]. In the application of porous membranes, fouling is one of the significant problems. Fortunately, in the gas-liquid contactor applications, the contactors are less sensitive to fouling since there is no convection flow through the membrane pores. However, pre-filtration is necessary for industrial application using hollow fibers with small diameters because gas and liquid streams with large content of suspending particles can cause plugging [3].

Although yet to be implemented industrially, the process has potential applications in various sectors. Supply and demand for fresh water have increased gradually in the last two decades. In this context, MD is a promising technology for desalting highly saline waters [14]. Other applications might be wastewater treatment [33], heavy metal removal [34], and the food industry. The primary interest has so far been water desalination [35]. Most of the current membrane distillation applications are still in the laboratory or small-scale pilot plant phase. The possibility of using renewable energy sources, such as waste heat, solar energy [36], [37], or geothermal energy, may enable membrane distillation to be integrated with other processes[1], making it a more promising separation process at an industrial scale [14], [32].

[1] With reverse osmosis [38], or to create an ultrafiltration unit [39].

4.1 Membrane Characteristics

Hydrophobic polymeric[2] porous membranes are used in the MD process. Membrane modules can be in various shapes: plate and frame, hollow fiber, tubular membrane, or spiral wound membrane. In general, membranes should be designed so that it has low resistance to mass transfer and low thermal conductivity to prevent heat loss across the membrane due to conduction. In addition, it should have good thermal stability in extreme temperatures and high resistance to chemicals [14]. Moreover, thermal and mechanical stability must be ensured to avoid degradation of the membrane during operation [5].

Membrane thickness δ also plays an important role. Both mass and heat fluxes are inversely proportional to δ. The dependence is the same in both cases, but the effects are different. For mass transfer, an increase of the thickness has a negative impact, and lower flux occurs. The growth has positively affects the heat transfer, i.e. a lower heat loss and a higher trans-membrane flux. For direct membrane configuration, optimal thickness is estimated between 30 and 60 μm [19].

MD is only possible if the restrictive condition is fulfilled that the pores of the membrane are not filled with liquid. In the membranes created by materials mentioned in previous paragraphs, the distillation of water and solutions of inorganic substances in water, the non-wetting condition is satisfied. In general, this is not the case for organic solutions [40].

To decide whether liquid penetrates the membrane pores, we define liquid entry pressure (LEP) as follows

$$\mathrm{LEP} = -\frac{2b\gamma_s \cos(\theta)}{r_{\max}}.$$

If the applied pressure exceeds value LEP, liquid penetrates the hydrophobic membrane. Thus MD can not be used. LEP value depends on the geometry of pores evaluated in b, γ_s is liquid surface tension, θ is a contact angle (see figure 4.1), and $r_{\max}$ is the maximum pore size [40].

The volume of the pores divided by the total volume of the membrane is called porosity, denoted by ε, densities of polymer material ρ_p and membrane ρ_m are calculated from measurements on pycnometer, and the porosity can be determined from Smolder-Franken equation [41]

$$\varepsilon = 1 - \frac{\rho_m}{\rho_p}.$$

Deviation of the pore structure from the cylindrical shape is called tortuosity, denoted by τ. The most successful correlation of porosity and tortuosity is suggested as [42]

$$\tau = \frac{(2-\varepsilon)^2}{\varepsilon}.$$

The permeate flux of water vapour j_v is proportional with porosity and inverse proportional with tortuosity and thickness of the membrane, the flux increases as $\overline{r}$ increases [20].

[2]Polytetrafluoroethylene (PTFE), polypropylene (PP), or polyvinylidene fluoride (PVDF) are often used.

4.2 Membrane Configurations

There are four basic process configurations in membrane distillation: direct contact membrane distillation, air gap membrane distillation, vacuum membrane distillation, and sweep gas membrane distillation [4]. Two new configurations named vacuum-multi-effect membrane distillation and permeate gap membrane distillation have also been tried recently [3].

4.2.1 Direct Contact Membrane Distillation (DCMD)

The hot solution is in direct contact with the hot membrane side surface in this configuration, see figure 4.2 a). Therefore, evaporation takes place at the feed-membrane surface. The vapour is moved by the pressure difference across the membrane to the permeate side and condenses inside the membrane module. Because of the hydrophobic characteristic, the feed cannot penetrate the membrane (only the gas phase exists inside the membrane pores). DCMD is the most straightforward MD configuration and is widely employed in desalination processes and concentration of aqueous solutions in food industries or acids manufacturing. The main drawback of this design is the heat lost by conduction [14]. A DCMD with a liquid gap (LGDCMD) is a DCMD variant in which a stagnant cold liquid is kept in direct contact with the permeate side of the membrane [32], see figure 4.2 b).

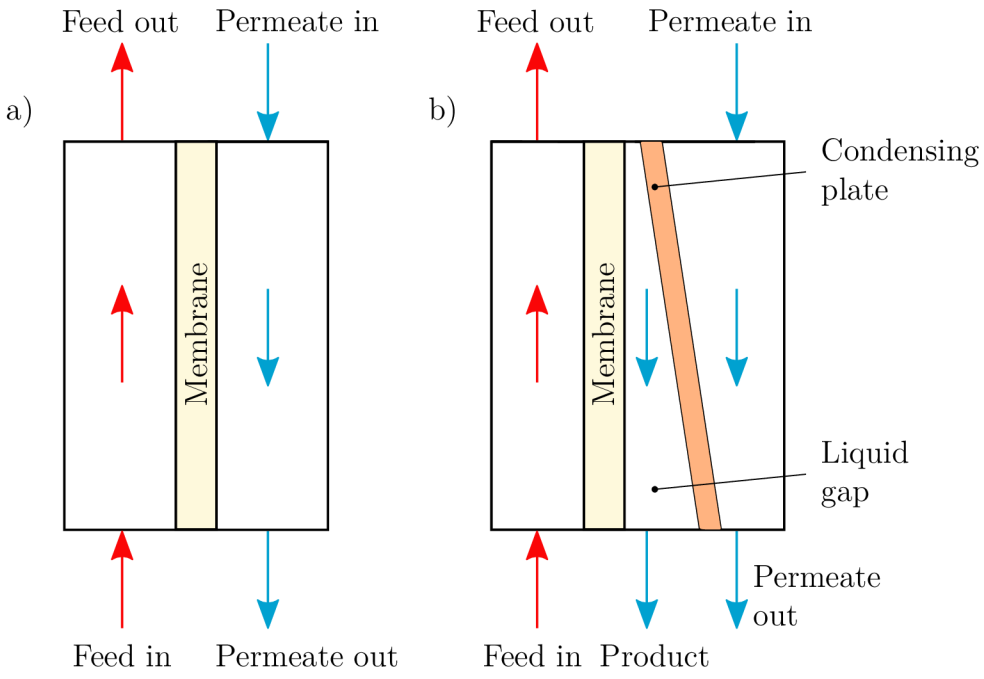

Figure 4.2: MD configurations. a) DCMD and b) LGDCMD membrane distillation configurations [4], [32].

4.2.2 Air Gap Distillation (AGMD)

Air gap distillation is a slight variation of direct contact membrane distillation, where a stagnant air gap is placed between the membrane and the condensation surface, which is placed in the module, see figure 4.3 a). The vapour molecules, therefore, move through both the membrane and the air gap before condensing. The air gap helps to reduce

the heat loss due to conduction. However, additional resistance is created that reduces the permeate flux. AGMD is considered the most flexible configuration, showing great promise for the future of membrane distillation. It is also more adaptable to the desalination of geothermal resources, with a lower energy requirement than DCMD [4].

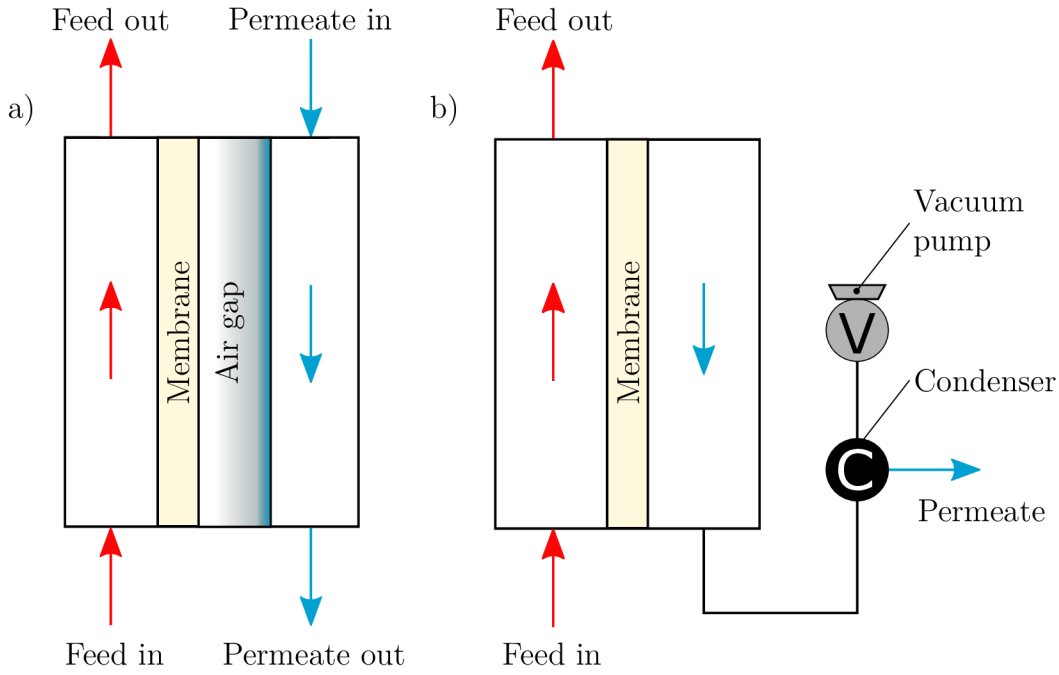

Figure 4.3: MD configurations. a) AGMD and b) VMD membrane distillation configurations. The gray object is a vacuum pump and the black object is a condenser [4], [32].

AMGD supplemented by a vacuum pump (V-AGMD) was developed to eliminate the air gap's disadvantage and improve the process performance. It was found that the vacuum pump could promote the permeate flux, thermal efficiency, gained output ratio, and performance ratio [43].

Permeate gap membrane distillation (PGMD) is another improvement of AGMD. The gap is being filled with water, the permeate water is separated from the coolant by a condensation surface, so the coolant can still be any type of liquid. The water in the gap can effectively reduce mass transfer resistance through the gap as vapour can immediately condense when leaving the membrane, like the DCMD, meanwhile with lower heat loss theoretically. Another benefit of PGMD compared to DCMD is the direct use of feed water as a coolant inside the module. Therefore, no external heat exchanger is needed to heat the feed before entering the pre-heating tank [44].

4.2.3 Vacuum Membrane Distillation (VMD)

The schematic diagram of this module is shown in figure 4.3 b). In VMD configuration, a pump is used to create a vacuum in the permeate membrane side. Condensation takes place outside the membrane module. The heat lost by conduction is negligible, which is considered a great advantage [20]. The benefit of reduced mass transfer resistance as diffusion is favoured at the liquid vapour interface. However, there is a disadvantage of increased risk of pore wetting [14], [32].

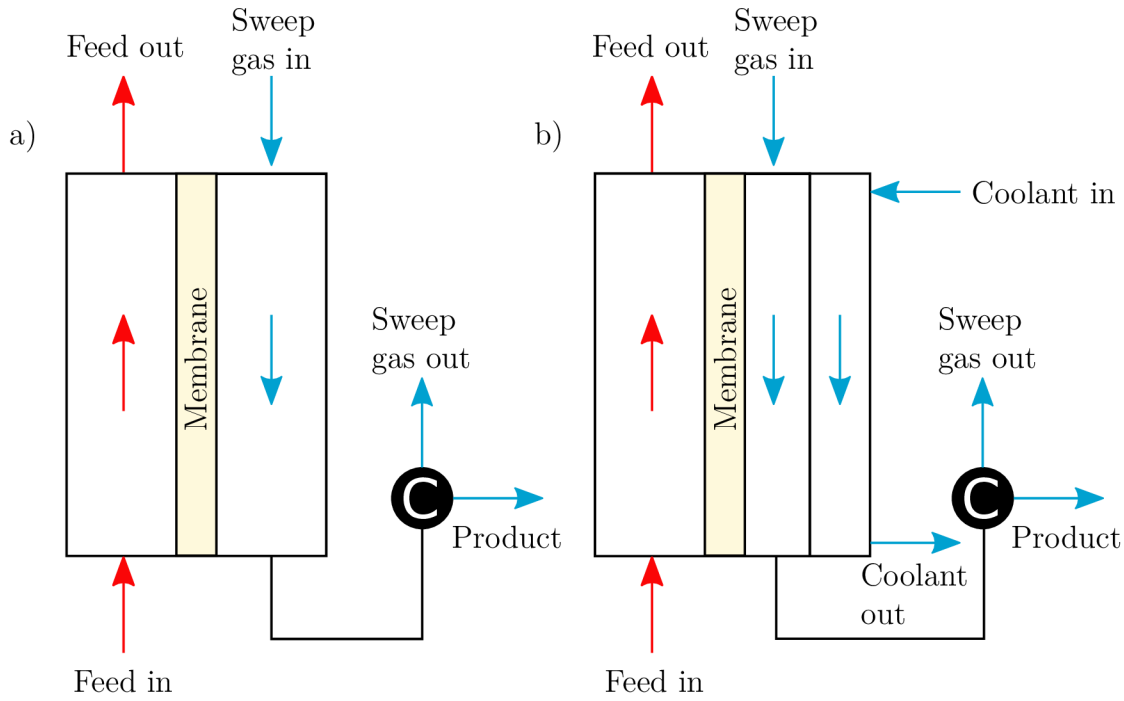

Figure 4.4: MD configurations. a) SGMD and b) TSGMD membrane distillation configurations. Black object is an condenser [4], [32].

4.2.4 Sweep Gas Membrane Distillation (SGMD)

As the name implies, sweep gas membrane distillation (SGMD) uses a cold inert gas to sweep the permeate side of the membrane carrying the vapour molecules, see figure 4.4 a). Similarly to AGMD, there is a gas barrier. Unlike stationary air in AGMD, sweep gas rather improves mass transfer. The condensation takes place outside the membrane module through the use of an external condenser. The main disadvantage of this configuration is that a small volume of permeate diffuses into a large sweep gas volume, thus requiring a large condenser [4]. In SGMD, the gas temperature, mass transport rate, and heat transfer rate change substantially during the course of the circulation of the inert sweep gas along the membrane module. Temperature change in the gas can be minimized using a cold surface on the permeate side of the membrane. This addition is a cross between the AGMD and SGMD, called thermostatic sweep gas membrane distillation (TSGMD), see figure 4.4 b) [32].

Due to low conductivity heat loss and improved mass transfer, SGMD seems to be a very promising distillation process that could move the current state of knowledge forward. Unfortunately, further development accompanies many problems e.g. turbulent behaviour of sweep gas, design of external condenser, optimizing operation conditions such as the temperature of sweep gas, speed of sweep gas. Moreover, SGMD has rarely studied configuration, i.e. about 6.4 % of the papers published up to January 2020 in refereed journals [45].

Therefore, a specific fully polymeric[3] SGMD unit developed by Heat Transfer and Fluid Flow Laboratory [46] is studied in further chapters.

[3]Bundles of polymeric hollow fibers form both the membrane module and the condenser.

5 PDE Model

MD is generally governed by a complex system of PDEs: continuity equation, the balance of momentum, energy, and humid equations.

5.1 Continuity Equation

The principle of conservation of mass is expressed as follows. Let Ω be a fixed volume. Then

$$\frac{\mathrm{d}}{\mathrm{d}t}\int_{\Omega}\rho(\mathbf{x},t)\,\mathrm{d}\mathbf{x} = -\int_{\Gamma}\rho(\mathbf{x},t)\mathbf{v}(\mathbf{x},t)\cdot\hat{\mathbf{n}}\,\mathrm{d}\Gamma, \tag{5.1}$$

that is, the rate of change of mass in a fixed volume Ω is equal to the mass flux through its surface Γ [47]. Applying divergence theorem (1.3), we can get from equation (5.1) well-known continuity equation

$$\frac{\partial\rho(\mathbf{x},t)}{\partial t} + \nabla\cdot(\rho(\mathbf{x},t)\mathbf{v}(\mathbf{x},t)) = 0.$$

For incompressible flow i.e. fluid density is a constant, we obtain

$$\nabla\cdot(\mathbf{v}(\mathbf{x},t)) = 0. \tag{5.2}$$

5.2 Balance of Momentum

For uniform fluid density and viscous flow, the balance of momentum can be deduced as

$$\frac{\partial\mathbf{v}}{\partial t} + (\mathbf{v}\cdot\nabla)\,\mathbf{v} = -\frac{1}{\rho}\nabla p + \nu\nabla\mathbf{v} + f, \tag{5.3}$$

where f are body forces, if they do not depend on the temperature, equations (5.2) and (5.3) constitute a closed system of equations concerning variables $\mathbf{v}$ and p called Navier–Stokes equations of viscous incompressible fluids with uniform density[1] [47].

5.3 Energy Equation

The first law of thermodynamics states that the increase of total energy (kinetic and internal energies) in a material volume is the sum of the heat transferred and the work done on the volume. Assuming uniform ρ, specific internal energy proportional to temperature, and that heat flux is expressed from Fourier's law (2.1). Energy equation can be derived as

$$c_r\left(\frac{\partial u}{\partial t} + \mathbf{v}\cdot\nabla u\right) = 2\nu\boldsymbol{T} : \boldsymbol{T} + \frac{\lambda}{\rho}\nabla\cdot\nabla u. \tag{5.4}$$

Constant occurring in dependency of internal energy on temperature is represented by c_r, $\boldsymbol{T}$ is the deformation tensor defined elementwise as

$$T_{ij} = \frac{1}{2}\left(\frac{\partial v_i}{\partial x_j} + \frac{\partial v_j}{\partial x_i}\right).$$

This tensor can be understood as a matrix with elements T_{ij}. Thus, the double dot operator in the equation (5.4) is coherent with the definition (1.2) [47].

[1] Shortly also known as Navier–Stokes equations.

5.4 Humid Equation

Change of phases occurs in the MD phenomena. Interaction between two species has to be described. For this purpose, humid equation of vapour phase is provided as

$$\frac{\partial (\rho\omega)}{\partial t} + \mathbf{v} \cdot \nabla (\rho\omega) = \nabla \cdot (D\rho\nabla\omega) ,$$

where ω is the humidity ratio [48].

5.5 Note on the PDE Model

We summarize the problem of membrane distillation modelling via PDE. We establish momentum, energy, and humid equations to the water side inside the membrane and continuity, momentum, energy, and humid equations to the air side. Boundary conditions are prescribed. Steady-state is supposed. Hence, all partial derivatives with respect to time are equal to zero, and no initial conditions are imposed.

As we can see, this model is the boundary value-problem of nonlinear second order PDE. It's common knowledge that similar equations are difficult to solve analytically. In particular, Navier-Stokes equations are known since the 19^{th} century. Though our understanding of them remains very limited, they are one of the unsolved Millennium Problems from Clay Mathematics Institute, see [49].

Practically, time-demanding software simulations are the only way to solve the provided boundary-value problem. Simulations can be done only on small parts of the system due to the complicated membrane and condenser geometry (figure 7.1). Unfortunately, fibers are distributed randomly. Thus, choosing a 'representant' part for modelling cannot be done easily. Even though we would have access to a super-computer such that imposing the whole geometry to a simulation software would be possible, just that would be probably more time demanding than doing an experiment in the laboratory. Therefore, the main effort of this work is to satisfactory describes MD using a less robust model. Nevertheless, it is worth mentioning the most recent work done by Li and Zhang focusing on crossflow shell-and-tube membrane configuration with regular spacing between fibers [50], [51], and a paper by Huang et al. studying the random distribution of fibers inside a shell [52].

6 Electrical Circuit Analogy Model

A one-dimensional mathematical model based on the analogy of transport phenomena with the electrical circuits is convenient for simplifying rather complicated problems. It also clarifies what mechanisms control heat and mass transfers and shows which parts are less important or even negligible.

6.1 Heat Transfer

Two main mechanisms occur in the MD system: conduction heat transfer $\dot{q}_c$ (across the membrane material and its gas-filled pores) and latent heat $\dot{q}_v$ (associated with the vapourized molecules). The influence of mass transfer on heat transfer can be ignored. We consider a steady-state operation. Both membrane and condenser are set up in the cross-flow arrangement to the tunnel with the sweeping gas. In this part, we discuss heat transfer only through the membrane. The heat transfer through the condenser is not important because it happens outside of the membrane and does not influence the phenomena inside the membrane directly. On the other hand, we pay attention to the condenser in the experimental part to evaluate whether it is efficient [4]. The heat transfer is described by three steps, as illustrated in figure 6.1:

(I) heat transfer through the feed boundary layer $\dot{q}_f$,

(II) heat transfer through the membrane $\dot{q}_m$,

(III) heat transfer through the permeate boundary layer $\dot{q}_a$.

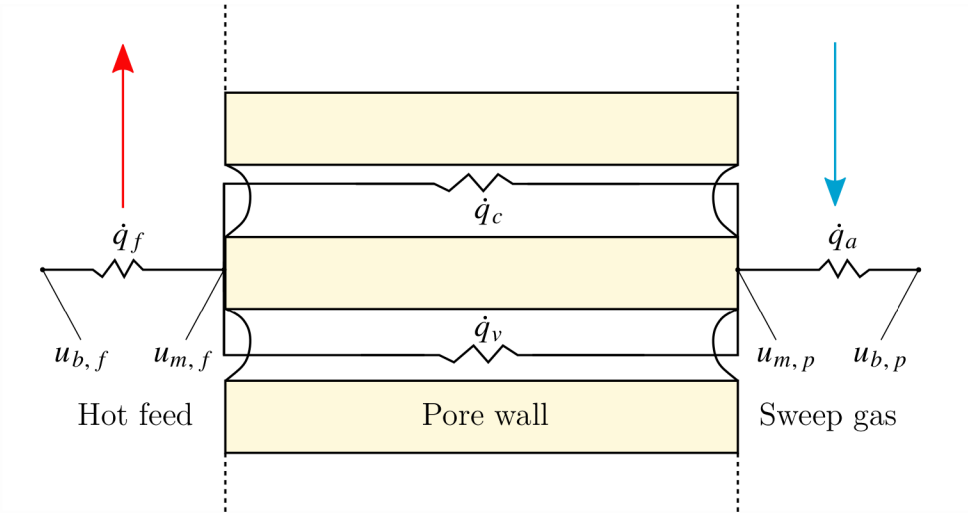

Figure 6.1: Heat transfer resistances in SGMD [4].

From the balance of energy, the heat transfer through the membrane is given as

$$\dot{q}_m = \dot{q}_c + \dot{q}_v = \frac{\lambda_m}{\delta}\left(u_{m,f} - u_{m,p}\right) + \sum_k j_k \Delta H_{v,k}, \tag{6.1}$$

where $\Delta H_{v,k}$ is the latent heat of evaporation of species k transported through the membrane pores with a transmembrane permeate flux j_k. Temperatures $u_{b,f}$, $u_{m,f}$ stand for the bulk temperatures of feed and permeate, $u_{m,f}$, and $u_{m,p}$ are the feed and permeate temperatures at the membrane surface, respectively.

If surface temperatures cannot be measured experimentally or calculated directly, the iterative model is used to estimate those temperatures as

$$u_{m,f} = u_{b,f} - \frac{\sum_k j_k \Delta H_{v,k} + \lambda_m \left(u_{m,f} - u_{m,p}\right) \delta^{-1}}{h_f^*} \quad \text{and}$$

$$u_{m,p} = u_{b,p} - \frac{\sum_k j_k \Delta H_{v,k} + \lambda_m \left(u_{m,f} - u_{m,p}\right) \delta^{-1}}{h_a^*}.$$

The latent heat of evaporation in the previous equations is computed at average membrane temperature. The logarithmic average can also be used [4], [53].

The thermal conductivity of the membrane λ_m can be estimated in several ways. Let λ_p and λ_g denote thermal conductivity of the membrane material and thermal conductivity of the gas filling the membrane pores, respectively. The most obvious relation is to take the weighted average in the following manner

$$\lambda_m = \varepsilon \lambda_g + (1 - \varepsilon) \lambda_p. \tag{6.2}$$

The previous equation (6.2) is called the isostrain model. Even though the weighted average makes physical sense, the isostress model in equation (6.3) provides much better agreement with real data [54],

$$\lambda_m = \left(\frac{\varepsilon}{\lambda_g} + \frac{(1 - \varepsilon)}{\lambda_p} \right)^{-1}. \tag{6.3}$$

Only latent heat is contributing to the positive outcome of MD. Conduction provides just heat loss. In SGMD configuration, up to 30 % of total heat transferred is lost due to conduction. We introduce thermal efficiency[1] η_{m} as [4]

$$\eta_{\mathrm{m}} = \frac{\dot{q}_v}{\dot{q}_v + \dot{q}_c} \cdot 100\ \%. \tag{6.4}$$

The overall transferred heat $\dot{q}$ can be expressed using the overall heat transfer coefficient as in equation (2.14). It should be equal to the heat transferred in each region (I), (II), and (III):

$$h \left(u_{b,f} - u_{b,p}\right) = \dot{q} = \dot{q}_f = \dot{q}_m = \dot{q}_a,$$

both heat fluxes through liquid and gas boundary layers are governed by Newton's cooling law (2.10), heat flux through the membrane is known from (6.1). Thus,

$$\dot{q} = h_f^* \left(u_{b,f} - u_{m,f}\right) = \frac{\lambda_m}{\delta} \left(u_{m,f} - u_{m,p}\right) + \sum_k j_k \Delta H_{v,k} = h_a^* \left(u_{m,p} - u_{b,p}\right). \tag{6.5}$$

Moreover, the overall heat transfer coefficient might be expressed as

$$h = \left(\frac{1}{h_f^*} + \frac{1}{\lambda_m \cdot \delta^{-1} + \sum_k j_k \Delta H_{v,k} \cdot \left(u_{m,f} - u_{m,p}\right)^{-1}} + \frac{1}{h_a^*} \right)^{-1}.$$

[1] Again with subscript 'm' we emphasize, that this effectiveness is different from one defined for heat exchangers in section 2.5.

When the air is used as the sweeping gas, and we suppose that there is no heat loss from the membrane to the surroundings, then the following relation holds

$$\dot{q} = \dot{q}_a = \frac{\dot{m}_a \left(i_{a,o} - i_{a,i}\right)}{A}. \tag{6.6}$$

The effective heat transfer area is denoted by A, $i_{a,o}$, and $i_{a,i}$ are specific enthalpies of moist air at the membrane module output and input respectively, which can be expressed from [4]

$$i_a = c_{h,a} u_a + \omega \Delta H_v^0 = \left(c_a + \omega c_{w,v}\right) u_a + \omega \Delta H_v^0. \tag{6.7}$$

where $c_{h,a}$ is the specific heat of the moist air with humidity ratio ω, the latent heat of evaporation ΔH_v^0 is taken at temperature 0 °C, c_a is the specific heat of the dry air, and $c_{w,v}$ is the specific heat of the water vapour. The humidity ratio inside the membrane might be expressed as [55]

$$\omega = \omega_i + \frac{j_v A}{\dot{m}_a}, \tag{6.8}$$

where ω_i is the humidity ratio of approaching moist air to the membrane module.

When only water vapour is transported through the membrane pores, equations (6.6)–(6.8) yield the equation for the heat transfer on the permeate side

$$\dot{q}_a = \frac{\dot{m}_a \left(c_a + \omega_i c_{w,v}\right) \left(u_{a,o} - u_{a,i}\right)}{A} + j_v \left(\Delta H_v^0 + c_{w,v} u_{a,o}\right).$$

The gas temperature along the membrane changes considerably. Hence, the previous approach should be applied only locally. Permeate flux is a function of position along the membrane module. The total permeate flux might be computed as integral along the membrane divided by the module length (mean value).

One of the limiting factors of SGMD efficiency is the heat transfer through the boundary layers. To express whether the membrane is well designed, we introduce local (global one can be again taken as a mean value) polarization coefficient ψ as

$$\psi = \frac{u_{m,f} - u_{m,p}}{u_{b,f} - u_{b,p}}. \tag{6.9}$$

This coefficient reflects the reduction of the driving force (vapour pressure difference), which negatively influences the process productivity. In the ideal case, the value should be equal to one. Usually, it is lower. For the DCMD module with polarization coefficient higher than 0.6 is considered to be designed well, the mass transfer resistance limits the process. On the other hand, values below 0.2 mean that the module has a poor design, and the distillation is limited by heat transfer. For SGMD, such specific numbers are not known yet. We add zero to the right side of equation (6.9) and rearrange it to obtain

$$\psi = \frac{u_{m,f} - u_{b,p}}{u_{b,f} - u_{b,p}} + \frac{u_{b,f} - u_{m,p}}{u_{b,f} - u_{b,p}} - 1. \tag{6.10}$$

If the heat transfer through the sweeping gas phase is very high, the temperatures $u_{m,p}$ and $u_{b,p}$ are very similar, so the second fraction in the equation (6.10) is close to unity. Thus, polarization effects in the liquid phase are important, so the SGMD process is

controlled by the heat transfer resistance of the feed layer and the mass transfer resistance of the membrane. On the other, if the heat transfer through the feed solution is very high, the temperatures $u_{m,f}$ and $u_{b,f}$ are very similar. Hence, first fraction in equation (6.10) is approaching one, so the gas phase is important for the temperature polarization effects. Therefore, the heat transfer resistance of the gas layer and the mass transfer resistance of the membrane control the SGMD process [4].

6.2 Mass Transfer

6.2.1 Theoretical Flux

One of the most important questions is how much permeate do we get from the module. In the case of SGMD with aqueous solutions as the feed containing nonvolatile solutes and using air as the sweep gas, so only vapourous water molecules are transported through the membrane pores, the theoretical answer is pretty straightforward. We introduce the overall mass transfer coefficient χ^* as the inverse of mass transfer resistance R_m including all mass resistances presented in figure 3.1. It can also be written as a function of the transmembrane pressure difference Δp_w:

$$j_v = \chi^* \Delta p = \chi \Delta p_w = \chi \left(p^0_{w,f} a_{w,f} - p_{w,p} \right), \tag{6.11}$$

where a_w is the activity of water[2], p is the partial pressure of water, superscript 0 means pure water, subscripts w, f, and p refer to water, feed, and permeate. Further, partial pressure of water on permeate side can be computed as

$$p_{w,p} = \frac{\omega P}{\omega + 0.622}, \tag{6.12}$$

where P is total pressure on the permeate side. Combining equations (6.8), (6.11), and (6.12), we obtain second order polynomial

$$j_v^2 + \left((\omega_i + 0.622) \frac{\dot{m}_a}{A} + \chi \left(P - p^0_{w,f} a_{w,f} \right) \right) j_v + \\ + \chi \frac{\dot{m}_a}{A} \left(P\omega_i - p^0_{w,f} a_{w,f} \left(\omega_i + 0.622 \right) \right) = 0 \tag{6.13}$$

Theoretical flux obtained from equation (6.13) is in good agreement with experimental data for shell-and-tube membrane when the mass transfer is assumed to be controlled by Knudsen and ordinary diffusions [4], [56].

6.2.2 Membrane Permeability

It is important to point out that the membrane permeability is an unknown parameter. Empiric formulas are known for the permeability of the three standard mass transfer mechanisms. Superscripts of permeability 'O', 'K', and 'P' stand for ordinary diffusion, Knudsen diffusion, and Poiseuille flow, respectively.

According to [14], ordinary diffusion is dominant if

$$K < 0.01 \text{ or } 100\ell < \overline{r}.$$

[2] Activity of water is the fraction of the partial water vapour pressure in the solution and the partial vapour pressure of pure water at the same temperature.

And the relation for the permeability is given as [55]

$$\chi^{\mathrm{O}} = \frac{D_{wv}}{uR}\frac{P}{p_a}\frac{\varepsilon}{\tau\delta}, \tag{6.14}$$

where D_{wv} is diffusivity coefficient between water and water vapour, p_a is the air pressure in the membrane pores. Fraction of p_a and P can be replaced with log mean mole fraction of air Y_{lm} [4],

$$Y_{\mathrm{lm}} = \frac{Y_{a,m,f} - Y_{a,m,p}}{\ln\left(Y_{a,m,f}Y_{a,m,p}^{-1}\right)}.$$

In the Knudsen region, the mean free path is large concerning membrane pore size. Molecule-pore wall collisions are dominant over the molecule-molecule collisions. The Knudsen mechanism prevails if [14]

$$K > 1 \text{ or } \ell > \overline{r}.$$

Then the permeability is reported as

$$\chi^{\mathrm{K}} = \frac{2}{3uR}\frac{\varepsilon\overline{r}}{\tau\delta}\sqrt{\frac{8uR}{\pi M_w}}, \tag{6.15}$$

where u is the absolute temperature, and R is the universal gas constant [55].

Poiseuille flow mechanism is dominant when the pore size is large in relation to the mean free path of the water molecules, molecule-molecule collisions prevail molecule-pore collisions, and total pressures on sides of the membrane are not similar. In this case, the membrane permeability is expressed as [55]

$$\chi^{\mathrm{P}} = \frac{\varepsilon\overline{r}^2}{\tau\delta}\frac{\overline{p}}{8\mu_w uR}. \tag{6.16}$$

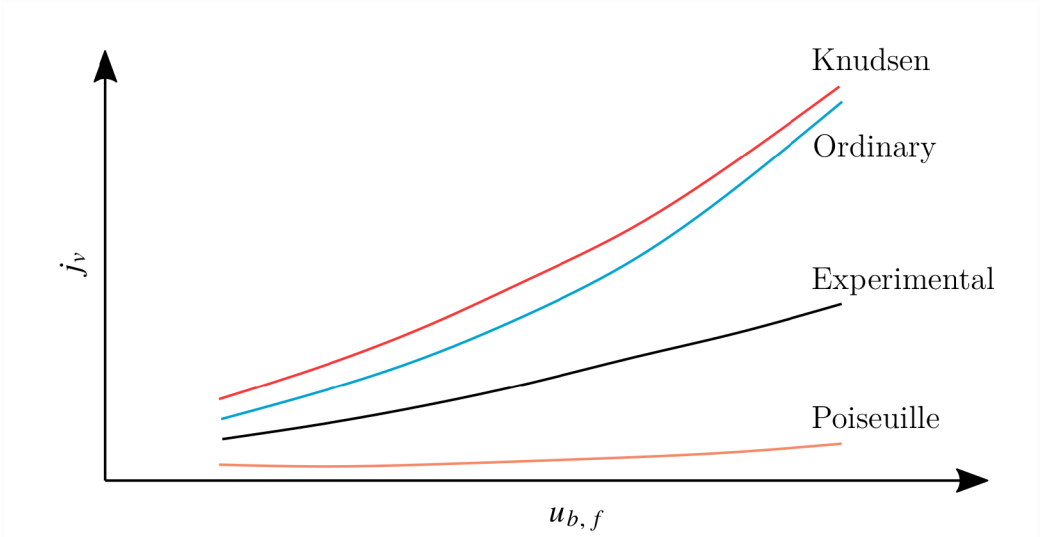

Figure 6.2: Comparison permeate flux for different mechanisms and experimental measurement with all variables fixed, but input feed temperature [4].

Comparison of predicted fluxes by presented mechanisms and experimental results often follow similar behaviour as presented in figure 6.2 [55]. For all variables fixed, except

input feed temperature. Knudsen and ordinary mass transfer predict higher permeate flux. On the other hand, Poiseuille expects much lower. Moreover, it can be concluded that the Poiseuille effect is negligible. Thus, mass transfer is modelled by Knudsen and ordinary mass transfer together. In the electrical circuit analogy (see figure 3.1), these two resistances lay in the series. Hence, the membrane permeability is given as

$$\chi^{\mathrm{KO}} = \left(\frac{1}{\chi^{\mathrm{K}}} + \frac{1}{\chi^{\mathrm{O}}} \right)^{-1}.$$

Poiseuille mass transfer shouldn't be excluded from the modelling if the size of pores is large, i.e. above 1µm [4], [29]. On the contrary, [57] provides the Knudsen-Poiseuille model working very well for smaller pores (0.1–0.45 µm). Again from electrical circuit analogy (see figure 3.1), we can easily write permeability including all three mechanisms [29]

$$\chi^{\mathrm{KOP}} = \left(\frac{1}{\chi^{\mathrm{K}}} + \frac{1}{\chi^{\mathrm{O}}} \right)^{-1} + \chi^{\mathrm{P}}. \tag{6.17}$$

7 Experiment

The SGMD is a promising distillation method that achieves the desired balance between reducing conductive heat loss and improving membrane permeability using flowing gas instead of condensing water and static air gap in the permeate side [37].

The experiment was done in Heat Transfer and Fluid Flow Laboratory. SGMD configuration with air as sweeping gas was used (7.2). Membrane input temperature was varied to 60, 70, and 80 °C. necessary physical quantities were measured to compute efficiency and performance.

7.1 Unit Description

The distillation unit consists of three main parts, the distillation tunnel containing the membrane module and the condenser [5].

Distillation tunnel forming rectangular 2000 mm × 1000 mm closed loop is made of transparent polycarbonate sheets so the process can be continuously observed. The tunnel's rectangular cross-section has 120 mm in height and 100 mm in width. Airflow in the tunnel is induced by a fan with a diameter of 100 mm with a supply voltage of 11 V. The speed of air inside the tunnel is 0.8 $m \cdot s^{-1}$.

The module membrane[1] in figure 7.1 a) consists of two bundles of 200 polymeric hollow fibers (PHF) with a length of 140 mm. It is made of hydrophobic polypropylene fibers with an outer diameter of 0.53 mm, an inner diameter of 0.44 mm. Hence, the membrane thickness δ is equal to 0.045 mm. Mass transport area is equal to 0.08 m^2. The average pore size is 0.1 µm with a porosity of 50 %, and LEP is higher than 350 kPa. Previous experiments showed [5] that fibers must be separated from each other to increase the permeate flux. It is done by pushing module terminals towards each other by 20 %, hydrophobicity is not affected, and no kinks are created by this method. The hot medium flowing through the membrane is modified with polyphosphate (0.02 $g \cdot l^{-1}$) to prevent fouling. Membrane input and output are placed on positions Tmi1 and Tmo1, respectively, see figure 7.2.

The polymeric hollow fibers heat exchanger (PHFHE) takes place as a condenser in the unit, see figure 7.1 b). It is also made of hydrophobic polypropylene. 200 PHFs of length 600 mm, outer diameter, and inner diameter of 0.8 mm and 0.6 mm respectively, create a chaotised[2] bundle with a total heat transfer area of 0.3 m^2. The condenser input and output are located in positions Tci1 and Tci2, respectively, see figure 7.2.

7.1.1 Measuring Devices

Input and output temperature, pressure drops, and water flow rate for the membrane module and the condenser were measured, i.e., at spots Tmi1 and Tmo1 for the membrane module and Tci2, Tco2 for the condenser. The humidity and temperature were measured inside the distillation tunnel on spots H1, H3, H4, and T1, T3, T4, respectively. Air speed was measured at H4.

Pt100 thermometers (OMEGA Engineering, Inc., Norwalk, CT, USA) with accuracy class 1/3DIN, i.e. error is (± 0.10+0.0017|u|) °C. The humidity meter (B+B Thermo-

[1] Company ZENA s.r.o. produced the membrane module [58].

[2] Chaotised PHFHE is used to guarantee that all fibers are in direct contact with the moist sweeping gas. A method of separation of PHFs is presented in [59].

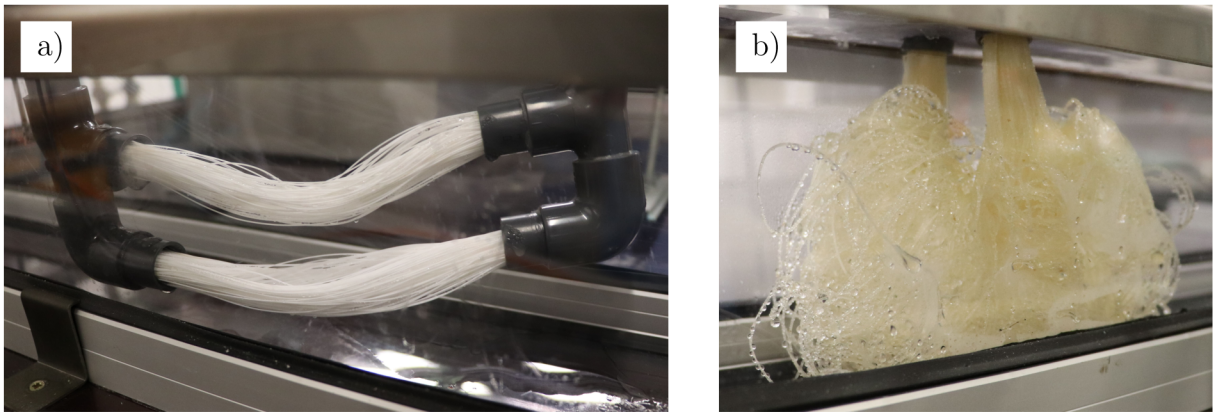

Figure 7.1: Detail in the distillation tunnel, a) membrane module and b) condenser.

Technik GmbH, Donaueschingen, Germany) gives an error of 3 % of the measured value relative humidity, the anemometer (OMEGA Engineering, Inc., Norwalk, CT, USA) has an accuracy of ± (5 % of measured value + 0.1) $m \cdot s^{-1}$, and the pressures (KELLER AG für Druckmesstechnik, Winterthur, Switzerland) are measured with an error of ± 25 Pa. The hot medium flow rate (ifm electronic, Essen, Germany) has an error of 0.4 $l \cdot min^{-1}$, and the flow rate through the condenser has an accuracy of ± 0.8 $l \cdot min^{-1}$.

7.1.2 Polymeric Hollow Fibers

It is well-known that polymers are not good heat conductors. Their thermal conductivity is usually between 0.1 and 0.4 $W \cdot m^{-1} \cdot K^{-1}$, which is 100–300 times lower than that of metals traditionally used for heat transport [17]. To increase the thermal conductivity by additives yield to overcome this disadvantage, e.g. adding graphite to polypropylene [60]. The idea for another solution comes from the analogy of heat transfer to electrical circuits. As we have seen, with decreasing wall thickness, the thermal resistance is decreasing. Thus, the transferred heat is increasing. For the condenser, the issue of low thermal conductivity is neglected due to the low thickness of the fibers' wall. For the membrane module. Low thermal conductivity is advantageous because it leads to low heat loss across the membrane due to the conduction.

Another drawback of PHF is the fouling phenomena, which can massively decrease both heat and mass transfer. It is also the main reason for undesirable leakage and damage to the membrane structure [61]. Internal fouling is dealt with by mechanical filtration and using water modified with polyphosphate, which causes the creation of the protective film on polymer material so that salt crystals are not fouling inside PHF. Water remains drinkable after using polyphosphate [5].

Besides some disadvantages, PHFs bring many benefits. Compared to the metal materials used for heat exchangers, polymers have higher chemical resistance, lower weight. It is much easier to shape them into various shapes [62]. Overall production requires less energy, and in addition, they are easy to recycle. Thus, PHFHEs are more environmentally friendly. Polymers offer high corrosion resistance. Hence, they can be used in the chemical industry and desalination [63], [64].

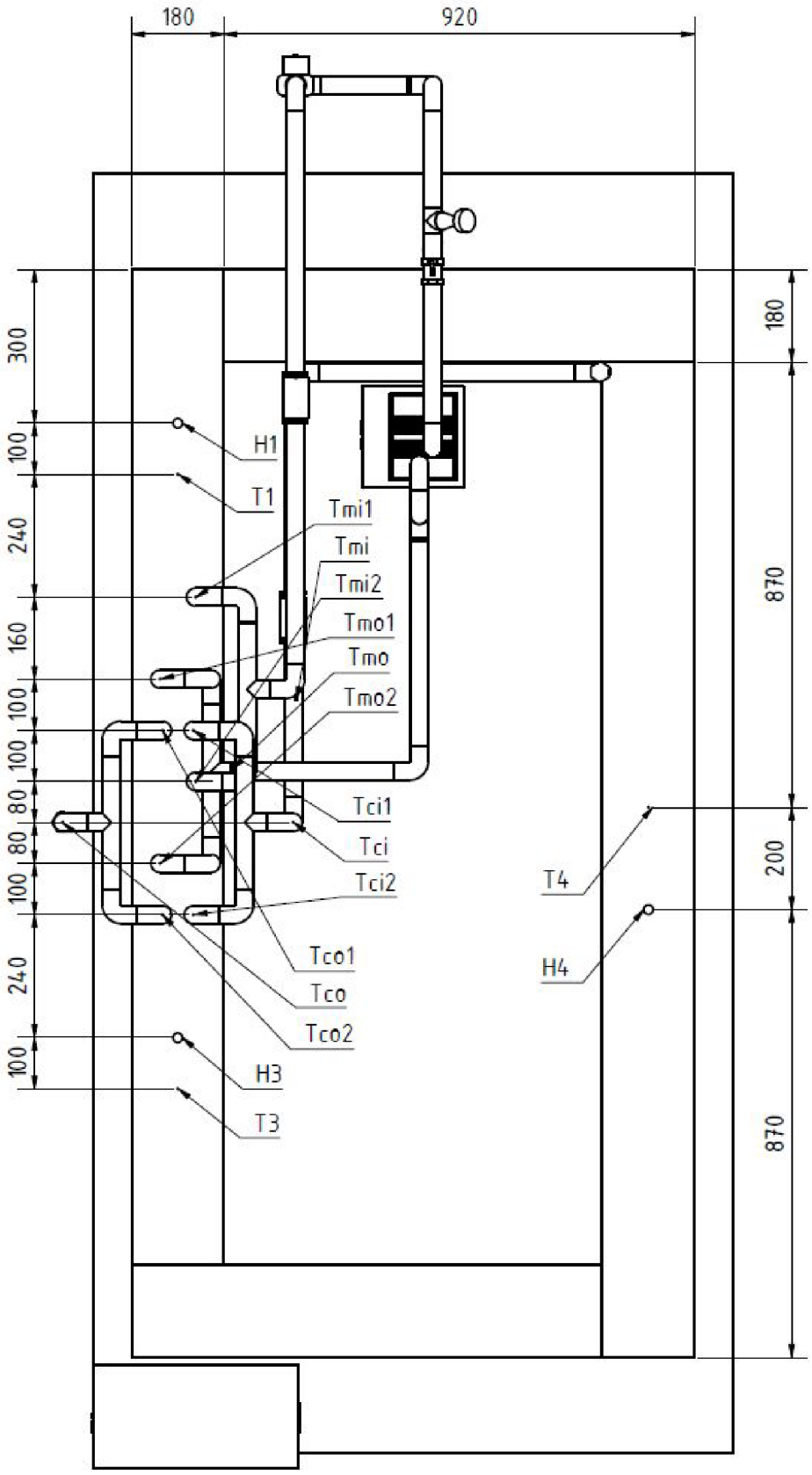

Figure 7.2: Scheme of the test rig, top view. Membrane module input and output are at positions Tmi1 and Tmo1 respectively, condenser input and output are located in Tci2 and Tco2 sequentially [5].

8 Results

The hot tap water modified with polyphosphate flows through the membrane module. It evaporates and its vapour leaves the membrane through pores. Then it is swept by air induced by a fan along the tunnel to the condenser, in which cold tap water flows. Air condensation occurs, and pure water is collected. For the clarity of subscript notation in the following sections, see table 8.1.

Table 8.1: Subscript notation.

Position	Description	Subscript
T1, H1	before membrane	1
Tmi1	membrane input	m, i
Tmo1	membrane output	m, o
	behind membrane	1a
	before condenser	2
Tci2	condenser input	c, i
Tco2	condenser output	c, o
T3, H3	behind condenser	3
T4, H4	opposite of membrane and condenser	4

It is worth noting that the Reynolds number of air inside the distillation tunnel was higher than 5000 for all experiments. Hence, turbulent and unsteady behaviour occurred. Data are time-averaged so that mean flow can be assumed as steady. Then flow can be treated as steady turbulent flow. To check whether data are time-averaged well, we check physical quantities of moist air in positions H1 and H4. Firstly, we suppose that mass flow rates of moist air are the same in both spots and compare computed mass flow rates of dry air[1]. Denote the relative error of computed rates by e_d. Secondly, we assume, that mass flow rates of dry air are identical in positions H1 and H4 and compare evaluated mass flow rates of moist air. Analogously, set e_m as the relative error in the evaluation. Both flow rate errors e_d and e_m do not exceed 0.1 % for studied measured data. It also tells us that surrounding air cannot access the distillation tunnel, and the condenser is good enough, i.e. evaporated water from the membrane condensates on the condenser and does not increase the moist air mass flow rate inside the tunnel.

Table 8.2: Measured temperature, relative humidity, and membrane mass flow rate during the experiment.

$u_{m,i}$ [°C]	$\dot{m}_m$ [l·h^{-1}]	$u_{m,o}$ [°C]	$u_{c,i}$ [°C]	$u_{c,o}$ [°C]	ξ_1 [%]	u_1 [°C]	ξ_3 [%]	u_3 [°C]	ξ_4 [%]	u_4 [°C]
60.33	65	59.31	11.34	11.68	82.13	20.35	93.83	17.23	82.92	19.23
70.09	80	68.15	11.58	12.04	89.25	21.76	95.25	18.54	88.66	18.54
80.06	65	77.46	11.08	11.68	98.50	21.52	97.79	18.98	98.26	20.46

The experiment was tested at the constant condenser mass flow rate of 100 l·h^{-1}. The water mass flow rate inside the membrane was either 65 or 80 l·h^{-1}. The speed of air inside the distillation tunnel was 0.8 m·s^{-1}, see measured data in table 8.2. Necessary

[1] Mass flow rate of dry air $\dot{m}_{a,d}$ is naturally defined as dry part of the mass flow rate of moist air as [12]

$$\dot{m}_{a,d} = \frac{\dot{m}_a}{1+\omega}.$$

properties of water and moist air were evaluated based on the measured temperatures as described in appendix A.

8.1 Membrane Module

From the first law of thermodynamics, the heat transfer rate through the membrane[2] is given as

$$q_m = \dot{m}_m c_m \left(u_{m,i} - u_{m,o}\right).$$

It was equal to 76 W for the lowest operating temperature. For the other two temperatures it was 166 W. Condensate was measured in ml·h^{-1} and recomputed to permeate flux j, it increased with increasing temperature on the membrane input, from 1.32 to 3.05 kg·h^{-1}·m^{-2}. The permeate flux was increased by 62 % after increasing temperature from 60 to 70 °C, whereas the heat transfer rate grew by 218 %. The highest temperature in the membrane input increased permeate flux by another 43 % with respect to the experiment with 70 °C at the membrane input, no change in heat transfer rate occurred. This indicates a problem. In fact, a higher mass flow rate induces higher pressure drop, thus, higher permeate flux. On the other hand, the heat transfer rate did not change. Therefore, the membrane efficiency, equation (6.4), rapidly decreased to circa 60 % in the experiment with 70 °C at the membrane input from around 80 % in the other experiments. This means that the second experiment is not directly comparable with the other two. See table 8.3 for the membrane module results.

Table 8.3: Membrane module, measured and evaluated data. Membrane input temperature, membrane mass flow rate, heat transfer rate, permeate flux, membrane pressure drop, membrane permeability, thermal effectiveness, and polarization coefficient.

$u_{m,i}$ [°C]	$\dot{m}_m$ [l·h^{-1}]	q_m [W]	j [kg · h^{-1} · m^{-2}]	Δp [kPa]	χ [mol · s · m^{-1} · kg^{-1}] ·10^6	η_m [%]	ψ [-]
60.33	65	76	1.32	30	2.16	79.35	0.27
70.09	80	166	2.14	42	1.70	59.22	0.35
80.06	65	166	3.05	30	1.22	85.35	0.32

Interpreting this result in the context of SGMD research is a quite difficult task because of many varying parameters such as membrane porosity, wall thickness, pore size, sweep gas speed, input temperatures, etc. In general, permeate flux ranges between 0.33 [65] and 22 kg·h^{-1}·m^{-2} [4], whereas pure water is used as solute. Similar modules are used in [5] varying permeate flux from 0.46 to 2.61 kg·h^{-1}·m^{-2}. It also suggests that permeate flux could be further improved by better fibers separation or using more condensers to reduce air humidity inside the tunnel.

The applied pressure was not higher than 150 kPa, which is much lower than liquid entry pressure. Therefore, the liquid could not penetrate the membrane pores. Thus, no undesirable leaks occurred. Membrane permeability was obtained from the definition (6.11) and was equal to 2.16·10^{-6}, 1.70·10^{-6}, and 1.22·10^{-6} mol · s · m^{-1} · kg^{-1} for membrane input temperatures 60, 70, and 80 °C sequentially. Knudsen number was higher than unity. Thus, the Knudsen diffusion is supposed to be the dominant mass transfer mechanism. The standard empiric permeabilities (6.14), (6.15), (6.16), and their combinations did not fit the evaluated values. The best agreement brings all three mechanisms (6.17), whereas the theoretical flux is approximately two times higher for all measured

[2] To be more precise, this is the rate of heat transfer that the moist air absorbs from the membrane.

temperatures. This indicates that the mass transfer surface could be used more efficiently. It also tells us that the standard empiric relations cannot be easily adapted for the studied PHF membrane module.

Reynolds number in the membrane did not exceed value 400. Thus, the flow is assumed to be fully developed laminar. The tube-side and air-side heat transfer coefficients were evaluated as proposed in section 2.6, from which necessary temperatures were determined to compute the polarization coefficient (6.9). In all cases, it was higher than 0.27. Thus, the distillation process was not limited by heat transfer. Moreover, temperatures $u_{m,f}$ and $u_{b,f}$ were very similar, i.e. at most 4 % relative difference, because the heat transfer through the feed is high. Therefore, the heat transfer resistance of the gas layer and the mass transfer resistance of the membrane control the process. To improve the performance, we propose to study the effect of the speed of sweeping gas. A higher speed should decrease the resistance of the gas layer and increase the pressure drop. On the other hand, it is necessary to keep the applied pressure below LEP.

8.2 Condenser

The heat transfer rate through the condenser[3] is computed as

$$q_c = \dot{m}_c c_c \left(u_{c,i} - u_{c,o}\right).$$

Its absolute value increased circa by one-third when the membrane input temperature was increased by 10 °C in both cases.

Studied condenser formed heat exchanger with crossflow arrangement. The logarithmic mean temperature difference method in section 2.4.2 was used to compute the overall heat transfer coefficient. The correction factor in equation (2.21) is equal to unity. The temperature of the hot medium, i.e. moist air, is assumed to be constant along the condenser. Its value is the dew point[4] of moist air entering the condenser. The effectiveness of the condenser was evaluated based on section 2.5. Both overall heat transfer coefficient and effectiveness have very low values, see table 8.4. The main reason is that the heat transfer area is too big. On the other hand, water vapour diffuses into a large sweep gas volume. Thus, it is necessary to use a large condenser. Another reason may

[3] Again, this is the heat transfer rate that the moist air gives to the condenser.

[4] Dew point $u_{k,d}$ of moist air in state k at constant pressure and specific humidity is a temperature to which moist air is cooled down to become saturated with water vapour. Further cooling causes condensation [12]. For the evaluation, we use mass and energy balance before and behind the condenser. The relative humidity is computed from the mass balance as

$$\xi_2 = \xi_3 + \frac{\dot{m}_w}{\dot{m}_{a,d}},$$

where $\dot{m}_w$ is measured mass flow rate of water. Specific enthalpy in '2' is given from energy balance as

$$i_2 = i_3 + \frac{\dot{m}_w i_w}{\dot{m}_{a,d}} - \frac{q_c}{\dot{m}_{a,d}},$$

i_3 and i_w are interpolated from measured data, see appendix A, then temperature u_2 is obtained from ξ_2 and i_2. Dew point is approximated as [67]

$$u_{2,d} \approx u_2 \left(1 - \frac{u_2 R \ln\left(\xi_2\right)}{\Delta H_v}\right)^{-1}.$$

be wrongly estimated dew point due to used measuring devices. The humidity meter can give an error of up to 3 % of measured relative humidity[5], which might play a significant role in determining the dew point. More precise devices should be used for further optimization of the condenser.

Table 8.4: Condenser, evaluated data. Membrane input temperature, heat transfer rate, overall heat transfer coefficient, and effectiveness.

$u_{m,i}$ [°C]	$\dot{m}_m$ [l·h^{-1}]	q_c [W]	h_c [W · m^{-2} · K^{-1}]	η_{he} [%]
60.33	65	-142	54.78	3.88
70.09	80	-193	64.04	4.53
80.06	65	-252	69.01	4.87

In water-air applications of heat exchangers such small overall heat transfer coefficient might be expected, [66] determined values between 25 and 55 W·m^{-2}·K^{-1} for finned-tube heat exchanger with water in tubes and air across tubes.

8.3 Overall Performance

The first thing one can realize is that the absolute heat transfer rate of the condenser is much higher than that of the membrane module. At first glance, it could mean that a fraction of power is somehow vanishing. However, the explanation is pretty simple. If we look at table 8.2, we see that relative humidities ξ_1 and ξ_3 are very similar, but temperatures u_1 and u_3 are significantly different. Thus, also specific enthalpies i_1 and i_3 notably differ. Therefore, the heat transfer rate of moist air from point '3' to '1' given as

$$q_{3,1} = \dot{m}_{a,d}\,(i_1 - i_3)\,,$$

is not negligible. To be more precise, power q_f due to the operation of the fan and heat transfer rate $q_{1\text{a},2}$ between membrane module and condenser should also be considered. Assume the following balance of energy of moist air in the tunnel

$$q_m + q_{1\text{a},2} + q_c + q_{3,1} + q_f = q_{\text{error}},$$

in the ideal case, the absolute thermal error q_{error} should be equal to zero. We also define a relative error e as a fraction of absolute thermal error and the sum of negative heat transfer rates in absolute value, i.e. absorbed heat by condenser and surroundings. The relative error does not exceed 4 %. Therefore, data are assumed to be precise enough. For details, see table 8.5.

Table 8.5: Specific enthalpies of moist air, joules are related to kilograms of dry air in the moist mixture, and relative thermal error of the system.

$u_{m,i}$ [°C]	i_1 [kJ · kg$_d^{-1}$]	$i_{1\text{a}}$ [kJ · kg$_d^{-1}$]	i_2 [kJ · kg$_d^{-1}$]	i_3 [kJ · kg$_d^{-1}$]	i_4 [kJ · kg$_d^{-1}$]	e [%]
60.33	52.30	58.31	58.53	47.01	49.14	2.27
70.09	59.72	72.70	73.36	51.46	55.32	2.46
80.06	63.39	73.48	77.12	52.81	59.09	3.73

[5]The measurement error is not further specified for relative humidity above 90 %.

9 Additional Data

Data from another three membrane modules were provided from the Heat Transfer and Fluid Flow Laboratory. Modules vary in the amount of fibers, and geometrical dimensions. Feed temperature and membrane mass flow rate are the only changing parameter during all the experiments for the specific membrane module. Every membrane is denoted by 'MM00X', where X is the number of hundreds of fibers in the module, see table 9.1.

Table 9.1: Membrane modules. Amount of fibers, overall mass transfer area, and air speed in the tunnel.

	Amount of fibers[2]	Mass transfer area [m^2]	v_a [$m \cdot s^{-1}$]
MM002	1×200	0.05	0.78
MM003	1×300	0.07	0.73
MM004[1]	2×200	0.08	0.80
MM006	2×300	0.15	0.73

[1]Membrane module studied in the previous chapters.
[2]'Number of bundles' × 'amount of fibers in one bundle'.

Membrane modules MM002 and MM003 consist of a single bundle of PHFs. The other two are created by two bundles. The identical condenser was used during all the experiments with the constant mass flow rate of 100 $l \cdot h^{-1}$, as described in section 7.1. Appendix B includes figures of the modules and condenser.

Data are evaluated in the same manner as the membrane module MM004 in section 8, see appendix C. Dependence of the permeate flux on the input feed temperature is shown in figure 9.1. It is worth noting that MM002 is the only module for which increasing feed temperature yields decreasing permeate flux.

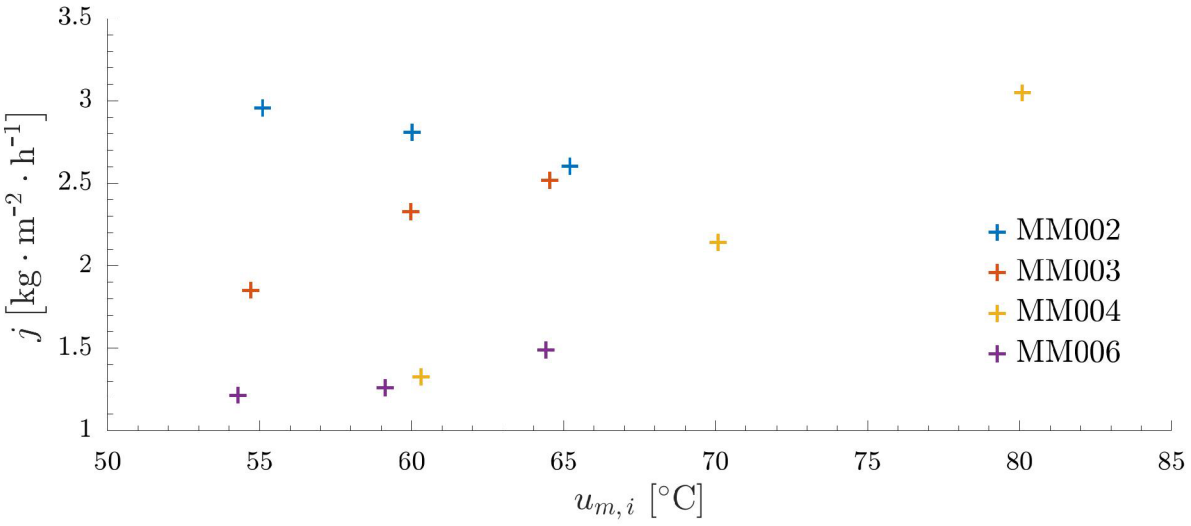

Figure 9.1: Measured dependence of permeate flux on the feed input temperature for membrane modules.

10 Permeate Flux Prediction

Running an experiment with a specific membrane input temperature for a particular module consumes a significant amount of time. Specifically, it can take up to one day in the laboratory. The 'measure-guess flux predictor' is built to speed up studying the fully polymeric distillation unit.

The conduction heat flux in equation (6.1) is not easily adaptable for PHFs. Some authors propose transforming the complicated geometrical system of PHFs into a flat sheet membrane and using the standard equations. This approach can be successfully adapted because of the regular fiber packing into a block and some geometrical parameters [68]. That is not the case with the studied modules in this work. Moreover, the great advantage of the shape flexibility is pulled out due to the suggested method.

Experimentally measured data showed that the permeate mass flow rate through the membrane is relatively low compared to the mass flow rate of water. Thus, the heat flux through the module is computed as

$$\dot{q}_m = \frac{\dot{m}_m c_m \left(u_{m,i} - u_{m,o}\right)}{A}.$$

We determine the overall heat transfer coefficient and membrane surface temperatures from (2.23)–(2.27) and (6.5), respectively. The definition of heat transfer rate gives $q_m = \dot{q}_m A$. From the first law of thermodynamics the heat transfer rate through the condenser is given as

$$q_c = \dot{m}_c c_c \left(u_{c,o} - u_{c,i}\right).$$

Specific enthalpies in spots '1', '3', and '4' are computed from measured data in the following way

$$i_k = \left(c_{a,k} + \omega_k c_{w,v,k}\right) u_k + \omega_k \Delta H_v^0, \text{ for } k = 1, 3, 4.$$

Specific enthalpies $i_{w,m}$ of water at temperature $u_{m,f}$ inside the membrane, and $i_{w,c}$ at the dew point determined from point '3' condensing at the condenser are interpolated as proposed in appendix A.

A positive permeate flux j is guessed. The mass and energy balance yields

$$i_{1\mathrm{a}} = i_1 + \frac{q_m}{\dot{m}_{a,d}} + \frac{jA}{\dot{m}_{a,d}} i_{w,m},$$
$$i_2 = i_3 - \frac{q_c}{\dot{m}_{a,d}} + \frac{jA}{\dot{m}_{a,d}} i_{w,c}.$$

If the following inequality holds

$$\frac{1}{|q_c|} > \left|\dot{m}_{a,d}\left(i_2 - i_{1\mathrm{a}}\right) + q_m + q_{3,4} + q_{4,1} + q_c + q_f\right|, \tag{10.1}$$

the predicted permeate flux is declared as the initial expected flux j_0 for the membrane at given conditions. Otherwise, another permeate flux is guessed. The process is being repeated until (10.1) is satisfied.

Once j_0 is known, we can easily find continuous interval I so that the condition (10.1) is fulfilled for all its elements. The midpoint of interval I is the predicted permeate flux by the measure-guess method.

10.1 Validation

The proposed measure-guess method is applied on time-averaged data from the first hour of the unit operation. For lower temperatures and membrane modules with a low number of fibers, the prediction works very well, i.e. the relative error is less than 5 %, see figure 10.1. The inaccuracy of the humid meter most likely causes this error. Better ther-

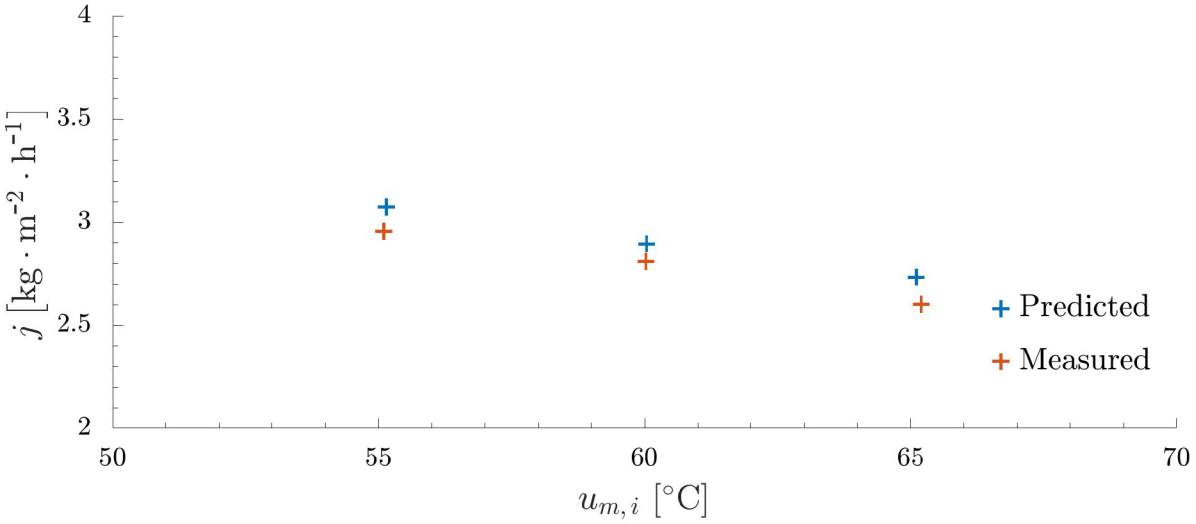

Figure 10.1: Measured and predicted dependence of permeate flux on the membrane input temperature, MM002.

mal isolation of the distillation tunnel between the membrane and condenser could also improve the precision of predictions.

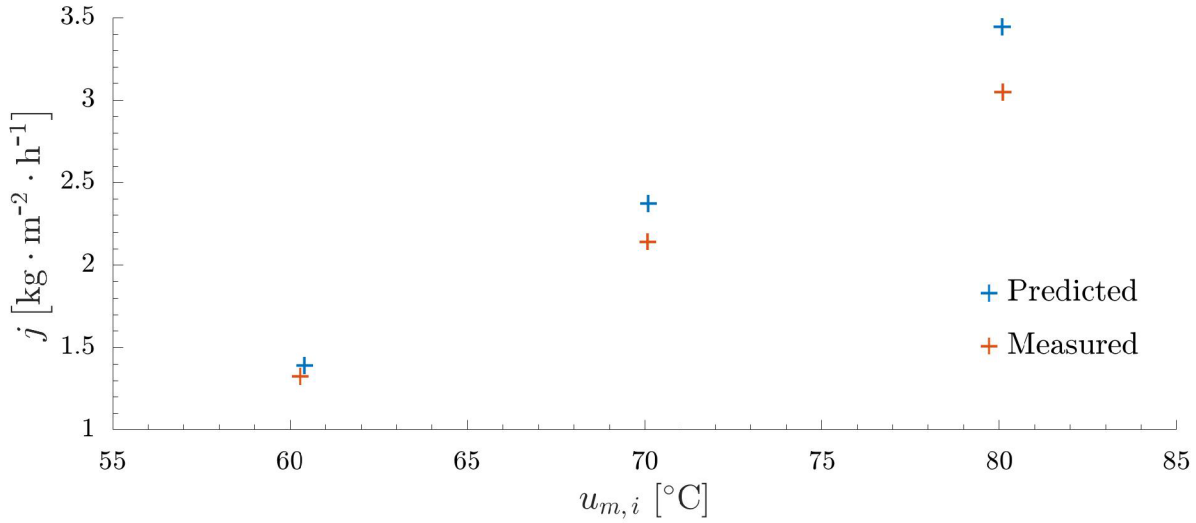

Figure 10.2: Measured and predicted dependence of permeate flux on the membrane input temperature, MM004.

In the case of higher temperatures or modules with high amount fibers, the prediction is exacerbated. The relative error of predicted and measured fluxes for MM004 is higher than 10 % at the input membrane temperature of 80 °C, see figure 10.2. The measured relative humidity in the whole distillation tunnel was higher than 90 % during this experiment. Thus, the error of the humidity meter might be higher than 3 %. Such error can change specific enthalpies significantly, which is leading to an inaccurate prediction.

Similar behaviour might be observed in membrane modules MM003 and MM006, see appendix D. The relative error of predictions is displayed in table C.1. To improve the data analysis and predictions, we propose to:

- use more precise humidity meters,
- decrease the relative humidity inside the distillation tunnel via using more condensers, operating at lower temperature, or utilizing membrane modules with fewer fibers.

Conclusion

Membrane distillation (MD), a relatively new process, is being investigated worldwide as a low cost and energy saving alternative to conventional separation methods. MD is a thermally driven process generally governed by the system of partial differential equations describing both mass and heat transfers. The problem is further complicated due to the complex geometry of polymeric hollow fibers utilized in the construction of the membrane module and turbulent behaviour of used sweeping air requiring a three-dimensional model. Practically, software simulations are the only suitable solution. On the other hand, they are very difficult to implement because of the vast and complex computational domain. This fact is also reflected in the low amount of articles in referred journals concerning this approach. Nevertheless, the necessary mathematical background, basic ideas, and recent important references are provided.

A less robust one-dimensional model is built using the analogy of transfer phenomena with the electrical circuits. Conduction and latent heat model the heat transfer, whereas the mass transfer is modelled by three dominant mechanisms, i.e. Knudsen diffusion, ordinary diffusion, and Poiseuille flow.

Polymeric hollow fibers were utilized to construct the alternative distillation unit in Heat Transfer and Fluid Flow Laboratory. Data were evaluated using the proposed one-dimensional model, properties of moist air, and the balance laws. Studied modules have high thermal efficiency. In most cases, at least 70 % of the provided heat transfer rate through the membrane contributes to the desired water evaporation.

The convective analysis shows that the mass transfer is not limited by the heat transfer through the membrane. On the other hand, it is controlled by the heat transfer resistance of the gas layer and the mass transfer resistance of the membrane. Thus, improvement can be made, specifically by increasing the mass flow rate of the sweeping gas. This must be done with caution because it also leads to a higher transmembrane pressure drop that cannot exceed the value 'liquid entry pressure'. Otherwise, the undesirable leakage of water inside the membrane pores occurs, damaging the membrane structure.

The permeate flux varies between 1.21 and 3.05 $\mathrm{kg \cdot m^{-2} \cdot h^{-1}}$. One of the highest values corresponds to the membrane module (referred as MM002 in main text) with the lowest amount of fibers that could be almost perfectly separated. This allows the mass area to be used more effectively. In all other membrane modules, the permeate flux is increased with increasing feed temperature. On the contrary, required power consumptions are usually also increased. The measurements indicate that the permeate flux strongly depends on fiber separation and proper segregation should be borne in mind. The best benefit ratio brings the MM002 with the input feed temperature of 60 °C. It distillates 2 l of pure water in 12 hours for the overall amount of energy around 3 kWh.

The standard theoretical flux proposed by the literature does not fit the experimentally measured data. In the best scenario, whereas the combined Knudsen-Ordinary-Poiseuille membrane permeability is assumed, the theoretical flux is approximately twice as big as the measured permeate flux. One of the explanations might be that provided membrane characteristics are not determined well enough. For instance, a small change of the porosity causes a notable change of the theoretical flux. The other explanation is that the permeability empiric relations cannot be directly adapted to the polymeric hollow fiber membrane modules.

The required time is the main bottleneck of the experiments. It is necessary to collect enough condensate to diminish errors caused by measurement and turbulent behaviour of the sweeping gas. In practice, a single datum is measured per day. To speed up

experiments, the 'measure-guess flux predictor' is built. The idea is very straightforward. All data are measured and permeate flux is guessed. If the energy and mass balances hold, guessed flux is declared as the expected flux. Otherwise, a new flux is guessed and the process is repeated until the balance laws hold. The extreme simplicity and good accuracy make this approach favourable over more rigorous models. In fact, the relative error is not higher than 5 % for lower operating temperatures if the predictor is used after one hour of running the experiment. On the other hand, for higher temperatures and modules with a big amount of fibers, a notable relative error is observed, i.e. above 10 %. It could be caused by the high error of humidity meter, especially when the relative humidity of moist air is above 90 %. Decreasing the humidity inside the unit or using more accurate measuring devices is proposed for more precise data evaluation and permeate flux prediction.

The presented alternative distillation unit requires further investigation. Particularly energy consumption, the effect of other operating parameters, and membrane characteristics. For this purpose, the measure-guess flux predictor can be used to speed up acquiring knowledge.

Bibliography

[1] *World Health Organization*. Drinking-water [online]. ©2021 WHO [cit. 20. 4. 2021]. Available at: https://www.who.int/news-room/fact-sheets/detail/drinking-water.

[2] KHAWAJI, Akili, D., KUTUBKHANAH, Ibrahim, K., and WIE, Jong-Mihn. Advances in seawater desalination technologies. *Desalination*. 2008, **221**(1-3), pp. 47-69. ISSN 0011-9164. DOI: 10.1016/j.desal.2007.01.067.

[3] DRIOLI, Enrico, ALI, Aamer, and MACEDONIO, Francesca. Membrane distillation: Recent developments and perspectives. *Desalination*. 2015, **356**, pp. 56-84. ISSN 0011-9164. DOI: 10.1016/j.desal.2014.10.028.

[4] KHAYET, Mohamed and MATSUURA, Takeshi. *Membrane Distillation Principles and Applications*. Amsterdam: Elsevier, 2011. ISBN 978-0-444-53126-1.

[5] KŮDELOVÁ, Tereza, BARTULI, Erik, STRUNGA, Alan, HVOŽĎA, Jiří, and DOHNAL, Miroslav. Fully Polymeric Distillation Unit Based on Polypropylene Hollow Fibers. *Polymers*. 2021, **13**(7). ISSN 2073-4360. DOI: 10.3390/polym13071031.

[6] FARLOW, Stanley J. *Partial differential equations for scientists and engineers*. Dover ed., 1st pub. New York: Dover Publ., 1993. Dover books on mathematics. ISBN 978-04-866-7620-3.

[7] EVANS, Lawrence C. *Partial differential equations*. 2nd ed. Providence: American Mathematical Society, 2010. ISBN 978-08-218-4974-3.

[8] FRANCŮ, Jan. *Parciální diferenciální rovnice*. Páté opravené vydání. Brno: Akademické nakladatelství CERM, 2017. ISBN 978-80-214-5577-1.

[9] MARSDEN, Jerrold E. and WEINSTEIN, Alan J. *Calculus III*. 2nd ed. New York: Springer-Verlag, 1985. ISBN 978-03-879-0985-1.

[10] BERGMAN, Theodor L., INCROPERA, Frank P., DEWITT, DAVID P., and LAVINE, Adrienne S. *Fundamentals of heat and mass transfer*. 7th ed. Hoboken: John Wiley & Sons, 2011. ISBN 978-0470-50197-9.

[11] ÖZISIK, M. Necati. *Heat Conduction*. 2nd ed. New York: John Wiley & Sons, 1993. ISBN 978-04-715-3256-9.

[12] PAVELEK, Milan. *Termomechanika*. Brno: Akademické nakladatelství CERM, 2011. ISBN 978-80-214-4300-6.

[13] HOF, Björn, et al. Experimental observation of nonlinear traveling waves in turbulent pipe flow. *Science*. 2004, **305**(5690), pp. 1594-1598. ISSN 0036-8075. DOI: 10.1126/science.1100393.

[14] ALKHUDHIRI, Abdullah, DARWISH, Naif, and HILAL, Nidal. Membrane distillation: A comprehensive review. *Desalination*. 2012, **287**, pp. 2–18. ISSN 0011-9164. DOI: 10.1016/j.desal.2011.08.027.

[15] BROŽOVÁ, Tereza. *Fázové změny na povrchu tepelných výměníků s dutými vlákny*. Brno, 2018. Dizertační práce. Vysoké učení technické v Brně, Fakulta strojního inženýrství, Laboratoř přenosu tepla a proudění.

[16] KROULIKOVÁ, Tereza, ASTROUSKI, Ilya, and RAUDENSKÝ, Miroslav. CHAOTISED POLYMERIC HOLLOW FIBRE BUNDLE AS A CROSSFLOW HEAT EXCHANGER IN AIR-WATER APPLICATION. *Acta Polytechnica*. 2020, **60**(4), pp. 318-323. DOI: 10.14311/AP.2020.60.0318.

[17] ZARKADAS, Dimitrios M. and SIRKAR, Kamalesh K. Polymeric hollow fiber heat exchangers: An alternative for lower temperature applications. *Industrial & engineering chemistry research*. 2004, **43**(25), pp. 8093-8106. ISSN 1520-5045. DOI: 10.1021/ie040143k.

[18] MCNAUGHT, A. D. and WILKINSON, A. *Compendium of Chemical Terminology*. 2nd ed. Oxford: Blackwell Scientific Publications, 1997. ISBN 0-967-85509-8.

[19] LAGANÀ, Fortunato, BARBIERI, Giuseppe, and DRIOLI, Enrico. Direct Contact Membrane Distillation: Modelling and Concentration Experiments. *Journal of Membrane Science*. 2000, **166**(1), pp. 1-11. ISSN 0376-7388. DOI: 10.1016/S0376-7388(99)00234-3.

[20] LAWSON, K. W. and LLOYD, D. R. Membrane distillation. I. Module design and performance evaluation using vacuum membrane distillation. *Journal of Membrane Science*. 1997, **120**(1) pp. 111-121. ISSN 0376-7388. DOI: 10.1016/0376-7388(96)00140-8.

[21] DATTA, R., DECHAPANICHKUL, S., KIM, J. S., FANG, L. Y., and UEHARA, H. A generalized model for the transport of gases in porous, non-porous, and leaky membranes. I. Application to single gases. *Journal of Membrane Science*. 1992, **75**(3), pp. 245-263. ISSN 0376-7388. DOI: 10.1016/0376-7388(92)85067-S.

[22] CURCIO, Efrem and DRIOLI, Enrico. Membrane Distillation and Related Operations—A Review. *Separation & Purification Reviews*. 2007, **34**(1), pp. 35-86. ISSN 1542-2127. DOI: 10.1081/SPM-200054951.

[23] KHAYET, Mohamed, VELÁZQUEZ, Armando, and MENGUAL, Juan I. Modelling mass transport through a porous partition: Effect of pore size distribution. *Journal of Non-Equilibrium Thermodynamics*. 2004, **29**(3), pp. 279-299. ISSN 1437-4358. DOI: 10.1515/JNETDY.2004.055.

[24] AL-OBAIDANI, Sulaiman, et al. Potential of membrane distillation in seawater desalination: Thermal efficiency, sensitivity study and cost estimation. *Journal of Membrane Science*. 2008, **323**(1), pp. 85-98 ISSN 0376-7388. DOI: 10.1016/j.memsci.2008.06.006.

[25] BIRD, Byron R., STEWART, Warren E., and LIGHTFOOT, Edwin N. *Transport phenomena.* 2nd ed. New York: John Wiley & Sons, 2002. ISBN 0-471-36474-6.

[26] HILMEN, Eva-Katrine. *Separation of Azeotropic Mixtures: Tools for Analysis and Studies on Batch Distillation Operation*. Trondheim, 2000. Doctoral dissertation. Norwegian University of Science and Technology, Department of Chemical Engineering.

[27] BANAT, Fawzi A., AL-RUB, Fahmi Abu, JUMAH, Rami, and AL-SHANNAG, Mohammad. Application of Stefan-Maxwell approach to azeotropic separation by

membrane distillation.*Chemical Engineering Journal*. 1999, **73**(1), pp. 71-75. ISSN 1385-8947. DOI: 10.1016/S1385-8947(99)00016-9.

[28] MALEK, Kourosh and COPPENS, Marc-Oliver. Knudsen self- and Fickian diffusion in rough nanoporous media. *Chemical Engineering Journal*. 2003, **119**(2801). ISSN 1385-8947. DOI: 10.1063/1.1584652.

[29] DING, Zhongwei, MA, Runyu, and FANE, A. G. A new model for mass transfer in direct contact membrane distillation. *Desalination*. 2003, **151**(3), pp. 217-227. ISSN 0011-9164. DOI: 10.1016/S0011-9164(02)01014-7.

[30] NAGY, Endre. *Basic Equations of Mass Transport Through a Membrane Layer*. 2nd ed. Amsterdam: Elsevier, 2018. ISBN 978-0-128-13723-9.

[31] BRUUS, Henrik. *Theoretical microfluidics* [online], lecture notes. 2004 Technical University of Denmark [cit. 20. 4. 2021]. Available at: http://homes.nano.aau.dk/lg/Lab-on-Chip2008_files/HenrikBruus_Microfluidics%20lectures.pdf.

[32] GORAK, Andrzej and SCHOENMAKERS, Hartmut. *Distillation: Operation and Applications.* 1st ed. Cambridge: Academic Press, 2014. ISBN 978-01-238-6876-3.

[33] ZOLOTAREV, P. P., UGROZOV, V. V., VOLKINA, I. B., and NIKULIN, V. M. Treatment of waste water for removing heavy metals by membrane distillation *Journal of Hazardous Materials*. 1994, **37**(1), pp. 77–82. ISSN 0304-3894. DOI: 10.1016/0304-3894(94)85035-6.

[34] GARCÍA-PAYO, M. C., IZQUIERDO-GIL, M. A., and FERNÁNDEZ-PINEDA C. Air gap membrane distillation of aqueous alcohol solutions. *Journal of Membrane Science*. 2000, **169**(1), pp. 61–80. ISSN 0376-7388. DOI: 10.1016/S0376-7388(99)00326-9.

[35] BANAT, Fawzi A. and SIMANDL, Jana. Desalination by membrane distillation: a parametric study. *Separation Science and Technology*. 1998, **33**(2), pp. 201-226. ISSN 1520-5754. DOI: 10.1080/01496399808544764.

[36] KUROKAWA, Hideaki and SAWA, Toshio. Heat recovery characteristics of membrane distillation. *Heat transfer-Japanese Research*. 1996, **25**(3), pp. 135–150. ISSN 1520-6556. DOI: 10.1002/(SICI)1520-6556(1996)25:3<135::AID-HTJ1>3.0.CO;2-Y.

[37] LI, Guopei, LU, Lin, and ZHANG, Li-zhi. System-scale modeling and membrane structure parameter optimization for solar-powered sweeping gas membrane distillation desalination system. *Journal of Cleaner Production*. 2020, **253**. ISSN 0959-6526. DOI: 10.1016/j.jclepro.2020.119968.

[38] CRISCUOLI, Alessandra and DRIOLI Enrico. Energetic and exergetic analysis of an integrated membrane desalination system. *Desalination*. 1999, **124**(1–3) pp. 243–249. ISSN 0011-9164. DOI: 10.1016/S0011-9164(99)00109-5.

[39] GRYTA, M., KARAKULSKI, K., and MORAWSKI, A. W. Purification of oily wastewater by hybrid UF/MD. *Water Research*. 2001, **35**(15), pp. 3665–3669. ISSN. DOI: 10.1016/S0043-1354(01)00083-5.

[40] FRANKEN, A. C. M., NOLTEN, J. A. M., MULDER, M. H. V., BARGEMAN, D., and SMOLDERS, C. A. Wetting criteria for the applicability of membrane distillation. *Journal of Membrane Science*. 1987, **33**(3), pp. 315-328. ISSN 0376-7388. DOI: 10.1016/S0376-7388(00)80288-4.

[41] SMOLDERS, K. and FRANKEN, A. C. M. Terminology for Membrane Distillation. *Desalination*. 1989, **72**(3), pp. 249-262. ISSN 0011-9164. DOI: 10.1016/0011-9164(89)80010-4.

[42] IVERSEN, S. B., BHATIA, V. K., DAM-JOHANSEN, K., and JONSSON, G. Characterization of microporous membranes for use in membrane contactors. *Journal of Membrane Science*. 1997, **130**(1-2), pp. 205-217 ISSN 0376-7388. DOI: 10.1016/S0376-7388(97)00026-4.

[43] ABU-ZEID, Mostafa Abd El-Rady, et al. Improving the performance of the air gap membrane distillation process by using a supplementary vacuum pump. *Desalination*. 2016, **384**, pp. 31-42. ISSN 0011-9164. DOI: 10.1016/j.desal.2016.01.020.

[44] CHENG, Lan, ZHAO, Yajing, LI, Pingli, LI, Wenlong, and WANG, Fang. Comparative study of air gap and permeate gap membrane distillation using internal heat recovery hollow fibre membrane module. *Desalination*. 2018, **426**, pp. 42-49. ISSN 0011-9164. DOI: 10.1016/j.desal.2017.10.039.

[45] SAID, Ibrahim A., CHOMIAK, Timothy, FLOYD, John, and LI, Qilin. Sweeping gas membrane distillation (SGMD) for wastewater treatment, concentration, and desalination: A comprehensive review. *Chemical Engineering and Processing-Process Intensification*. 2020, **153**. ISSN 0255-2701. DOI: 10.1016/j.cep.2020.107960.

[46] Heat Transfer and Fluid Flow Laboratory, [online]. ©2018 Heat Transfer and Fluid Flow Laboratory [cit 20. 4. 2021]. Avaialable at: https://www.heatlab.cz/.

[47] ŁUKASZEWICZ, Grzegorz and KALITA, Piotr. *Navier–Stokes Equations An Introduction with Applications*. New York: Springer International Publishing, 2016. ISBN 978-3-319-27758-5.

[48] FAGHRI, Amir and ZHANG, Yuwen. *Transport Phenomena in Multiphase Systems*. Amsterdam: Elsevier, 2006. ISBN 978-0-12-370610-2.

[49] *Clay Mathematics Institute*, Navier–Stokes Equation [online]. ©2021 Clay Mathematics Institute [cit. 20. 4. 2021]. Available at: https://www.claymath.org/millennium-problems/navier%E2%80%93stokes-equation.

[50] LI, Guo-Pei and ZHANG, Li-Zhi. Three-dimensional turbulent flow and conjugate heat and mass transfer in a cross-flow hollow fiber membrane bundle for seawater desalination. *International Journal of Heat and Mass Transfer*. 2018, **120**, pp. 328-341. ISSN 0017-9310. DOI: 10.1016/j.ijheatmasstransfer.2017.12.044.

[51] LI, Guo-Pei and ZHANG, Li-Zhi. Laminar flow and conjugate heat and mass transfer in a hollow fiber membrane bundle used for seawater desalination. *International Journal of Heat and Mass Transfer*. 2017, **111**, pp. 123-137. ISSN 0017-9310. DOI: 10.1016/j.ijheatmasstransfer.2017.03.107.

[52] HUANG, Si-Min, et al. Heat and mass transfer in a hollow fiber membrane contactor for sweeping gas membrane distillation. *Separation and Purification Technology*. 2019, **220**, pp. 334-344. ISSN 1383-5866. DOI: 10.1016/j.seppur.2019.03.046.

[53] TERMPIYAKUL, P., JIRARATANANON, Ratana, and SRISURICHAN, Surapit. Heat and mass transfer characteristics of a direct contact membrane distillation process for desalination. *Desalination*. 2005, **177**(1-3), pp. 133-141. DOI: 10.1016/j.desal.2004.11.019.

[54] PHATTARANAWIK, Jirachote, JIRARATANANON, Ratana, and FANE, Anthony G. Heat transport and membrane distillation coefficients in direct contact membrane distillation. *Journal of membrane science*. 2003, **212**(1-2), pp. 177-193. DOI: 10.1016/S0376-7388(02)00498-2.

[55] KHAYET, Mohamed, GODINO, Paz, and MENGUAL, Juan I. Nature of flow on sweeping gas membrane distillation. *Journal of membrane science*. 2000, **170**(2), pp. 243-255. DOI: 10.1016/S0376-7388(99)00369-5.

[56] KHAYET, Mohamed, GODINO, M. P., and MENGUAL, J. I. Theoretical and experimental studies on desalination using the sweeping gas membrane distillation method. *Desalination*. 2003, **157**(1-3) pp. 297-305. DOI:10.1016/S0011-9164(03)00409-0.

[57] SCHOFIELD, R. W., FANE, A. G., and FELL, C. J. D. Gas and vapour transport through microporous membranes. I. Knudsen-Poiseuille transition. *Journal of Membrane Science*. 1990, **53**(1-2), pp. 159-171. DOI: 10.1016/0376-7388(90)80011-A.

[58] ZENA MEMBRANES, [online]. ©2015 zena-membranes.cz [cit. 20. 4. 2021]. Available at: http://www.zena-membranes.cz/.

[59] RAUDENSKÝ, Miroslav, ASTROUSKI, Ilya, and DOHNAL, Miroslav. Intensification of heat transfer of polymeric hollow fiber heat exchangers by chaotisation. *Applied Thermal Engineering*. 2017, **113**, pp. 632-638. ISSN 1359-4311. DOI: 10.1016/j.applthermaleng.2016.11.038.

[60] QIN, Yuchun, LI, Baoan, and WANG, Shichang. Experimental investigation of a novel polymeric heat exchanger using modified polypropylene hollow fibers. *Industrial & engineering chemistry research*. 2012, **51**(2), pp. 882-890. ISSN 1520-5045. DOI: 10.1021/ie202075a.

[61] NAIDU, Gayathri, et al. A review on fouling of membrane distillation. *Desalination and water treatment*. 2016, **57**(22), pp. 10052-10076. ISSN 1944-3986. DOI: 10.1080/19443994.2015.1040271.

[62] CHEN, Xiangjie, SU, Yuehong, REAY, David, and RIFFAT, Saffa. Recent research developments in polymer heat exchangers–A review. *Renewable and Sustainable Energy Reviews*. 2016, **60**, pp. 1367-1386. ISSN 1364-0321. DOI: 10.1016/j.rser.2016.03.024.

[63] BARTULI, Erik, KŮDELOVÁ, Tereza, and RAUDENSKÝ, Miroslav. Shell- and-tube polymeric hollow fiber heat exchangers with parallel and crossed fibers. *Applied Thermal Engineering*. 2021, **182**. ISSN 1359-4311. DOI: 10.1016/j.applthermaleng.2020.116001.

[64] SCHORR, Michael, VALDEZ, Benjamín, ELIEZER, Amir, SALINAS, Ricardo, and LORA, Carlos. Managing corrosion in desalination plants. *Corrosion Reviews*. 2019, **37**(2), pp. 103-113. ISSN 2191-0316. DOI: 10.1515/corrrev-2018-0038.

[65] ABEJÓN, Ricardo, SAIDANI, Hafedh, DERATANI, André, RICHARD, Christophe, and SÁNCHEZ-MARCANO, José. Concentration of 1, 3-dimethyl-2-imidazolidinone in Aqueous Solutions by Sweeping Gas Membrane Distillation: From Bench to Industrial Scale. *Membranes*. 2019, **9**(12). ISSN 2077-0375. DOI: 10.3390/membranes9120158.

[66] HOLMAN, Jack Philip *Heat Transfer*. 10th edition. New York: McGraw Hill, 2010. ISBN 978-0-073-52936-3.

[67] LAWRENCE, Mark G. The relationship between relative humidity and the dewpoint temperature in moist air: A simple conversion and applications. *Bulletin of the American Meteorological Society*. 2005, **86**(2), pp. 225-234. ISSN 1520-0477. DOI: 10.1175/BAMS-86-2-225.

[68] LI, Guopei and LU, Lin. Modeling and performance analysis of a fully solar-powered stand-alone sweeping gas membrane distillation desalination system for island and coastal households. *Energy Conversion and Management*. 2020, **205**. ISSN 0196-8904. DOI: 10.1016/j.enconman.2019.112375.

[69] BORGNAKKE, Claus, and SONNTAG, Richard E. *Fundamentals of Thermodynamics*. 8th ed. New York: John & Sons, 2013. ISBN 978-1-118-65286-2.

List of Figures

List of Tables

List of Symbols

SYMBOL	UNIT	MEANING
A	[m^2]	Area
a	[-]	Activity of water
b	[m]	Pore geometry parameter
C	[$J \cdot K^{-1}$]	Specific heat
c	[$J \cdot kg^{-1} \cdot K^{-1}$]	Specific heat capacity
c	[-]	Constant
D	[$m^2 \cdot s^{-1}$]	Binary mass diffusivity
d	[m]	Diameter
E	[J]	Emisive power
e	[-]	Relative error
F	[-]	Correction factor
f	[—]	Function, body forces function
h	[$W \cdot m^{-2} \cdot K^{-1}$]	Overall heat transfer coefficient
h^*	[$W \cdot m^{-2} \cdot K^{-1}$]	Convective heat transfer coefficient
I	[—]	Interval
i	[$J \cdot kg^{-1}$]	Specific enthalpy
$\mathbf{j}$	[$kg \cdot s^{-1} \cdot m^{-2}$, $mol \cdot s^{-1} \cdot m^{-2}$]	Permeate flux, mass flux
K	[-]	Knudsen number
k	[$m^2 \cdot kg \cdot s^{-2} \cdot K^{-1}$]	Boltzmann constant
L	[m]	Characteristic length, length
ℓ	[m]	Mean free path
M	[$kg \cdot mol^{-1}$]	Molecular weight
m	[kg]	Mass
$\dot{m}$	[$kg \cdot s^{-1}$]	Mass flow rate
$\mathbf{N}$	[$mol \cdot s^{-1} \cdot m^{-2}$]	Cumulative molar flux
N	[-]	Number of transfer units
Nu	[-]	Nusselt number
$\hat{\mathbf{n}}$	[—]	Unit normal vector
P	[Pa]	Total pressure on the permeate side
p	[Pa]	Pressure
q	[W]	Heat transfer rate
$\dot{q}$	[$W \cdot m^{-2}$]	Heat flux
q'	[$W \cdot m^{-3}$]	Rate of energy per unit volume
R	[$J \cdot K^{-1} \cdot mol^{-1}$]	Universal gas constant
Re	[-]	Reynolds number
r	[m]	Radius, pore size

$\boldsymbol{T}$	[Pa]	Deformation tensor
t	[s]	Time
u	[°C, K]	Temperature
$\mathbf{v}$	[m·s^{-1}]	Velocity vector
W	[—]	Control volume
$\mathbf{x}$	[—]	Vector of variables $x_1, x_2, \ldots x_n$
Y	[-]	Molar fraction
y	[mol·m^{-3}]	Molar concentration
ΔH	[J · kg^{-1}]	Latent heat
Δp	[Pa]	Pressure drop
Δu	[°C, K]	Temperature difference
$\boldsymbol{\alpha}$	[—]	Vector of multiindices $\alpha_1, \ldots \alpha_n$
Γ	[—]	Boundary of an open subset $\boldsymbol{\Omega}$
γ	[Pa]	Liquid tension
δ	[m]	Boundary layer width, wall thickness
ε	[-]	Porosity
η	[-]	Efficiency
θ	[rad]	Contact angle
λ	[W·m^{-1}·K^{-1}]	Thermal conductivity
μ	[Pa·s]	Dynamic viscosity
ν	[m^2·s^{-1}]	Kinematic viscosity
ξ	[-]	Relative humidity
ρ	[kg·m^{-3}]	Density
σ	[W·m^{-2}·K^{-4}]	Stefan-Boltzmann constant
τ	[-]	Tortuosity
χ	[mol · s · m^{-1} · kg^{-1}]	Membrane permeability
χ^*	[mol · s · m^{-1} · kg^{-1}]	Overall mass transfer coefficient
ψ	[-]	Polarization coefficient
$\boldsymbol{\Omega}$	[—]	Open subset of $\mathbb{R}^n$
ω	[kg · kg^{-1}]	Humidity ratio

SUBSCRIPT	MEANING
a	Air
b	Bulk
C	Crossflow
CF	Counterflow
c	Conduction, critical, cold liquid, condenser
d	Dry air

error	Thermal error
f	Feed, fan
g	Gas
h	Hot liquid
he	Heat exchanger
i	Input, i-th position
j	j-th position
k	Index
lm	Logarithmic mean
m, m	Membrane module
max	Maximal
min	Minimal
n	Normal direction
o	Output, overall
p	Permeate, polymer material
r	Dependency of internal energy on temperature
s	Surface
u	Thermal
v	Vapour, velocity, evaporation
w	Water
1	At point 1, body 1, left end of a heat exchanger
1a	At point 1a
2	At point 2, body 2, right end of a heat exchanger
3	At point 3
4	At point 4
∞	Free stream condition

SUPERSCRIPT	MEANING
K	Knudsen diffusion
O	Ordinary diffusion
P	Poiseuille flow
0	At 0 °C, pure water, initial

OVERBAR	MEANING
$\overline{}$	Mean value

List of Abbreviations

Abbreviation	Meaning
AGMD	Air gap membrane distillation
DCMD	Direct contact membrane distillation
HTC	Overall heat transfer coefficient
LEP	Liquid entry pressure
LGDCMD	Liquid gap direct contact membrane distillation
MD	Membrane distillation
MM00X	Membrane module with X hundreds of fibers
PDE	Partial differential equation
PGMD	Permeate gap membrane distillation
PHF	Polymeric hollow fiber
PHFHE	Polymeric hollow fiber heat exchanger
PP	Polypropylene
PTFE	Polytetrafluoroethylene
PVDF	Polyvinylidene fluoride
SGMD	Sweep gas membrane distillation
TSGMD	Thermostatic sweep gas membrane distillation
VMD	Vacuum membrane distillation

Appendices

A Thermophysical Properties

The properties at atmospheric pressure of moist and dry air were interpolated from tables in [69] and [10], respectively. Enthalpy of water was interpolated from [69], other properties of water were considered to be only temperature-dependent, whereas the temperature in °C was taken as the average of temperatures on the input and output of the system (i.e. of the membrane module or the condenser) [16]. The dynamical viscosity:

$$\mu = \exp\left(-6.358 - 2.88 \cdot 10^{-2} u + 1.31 \cdot 10^{-4} u^2 - 2.58 \cdot 10^{-7} u^3\right) \qquad [\mathrm{Pa} \cdot \mathrm{s}]\,,$$

the specific heat capacity:

$$c_p = 1.3410^{-9} u^6 - 4.9506 \cdot 10^{-7} u^5 + 7.09647 \cdot 10^{-5} u^4 - 0.004864569 u^3 - \\ - 0.16759809 u^2 - 2.81027645351 u + 4201.37207 \qquad \left[\mathrm{J} \cdot \mathrm{K}^{-1} \cdot \mathrm{kg}^{-1}\right],$$

the thermal conductivity:

$$\lambda = 5.76 \cdot 10^{-1} + 1.77 \cdot 10^{-3} u - 6.37 \cdot 10^{-6} u^2 \qquad \left[\mathrm{W} \cdot \mathrm{K}^{-1} \cdot \mathrm{m}^{-1}\right],$$

the density:

$$\rho = 1001 - 0.0672 u - 4.04 \cdot 10^{-3} u^2 + 4.94 \cdot 10^{-6} u^3 \qquad \left[\mathrm{kg} \cdot \mathrm{m}^{-3}\right],$$

the latent heat of evaporation:

$$\Delta H_v = 1918460 \left(\frac{u + 273.15}{u + 273.15 - 33.91}\right)^2 \qquad \left[\mathrm{J} \cdot \mathrm{kg}^{-1}\right].$$

B Figures

Figure B.1: Single-bundle membrane module MM003 [5].

Figure B.2: Double-bundle membrane module MM006 [5].

Figure B.3: Polymeric hollow fiber heat exchanger, condenser [5].

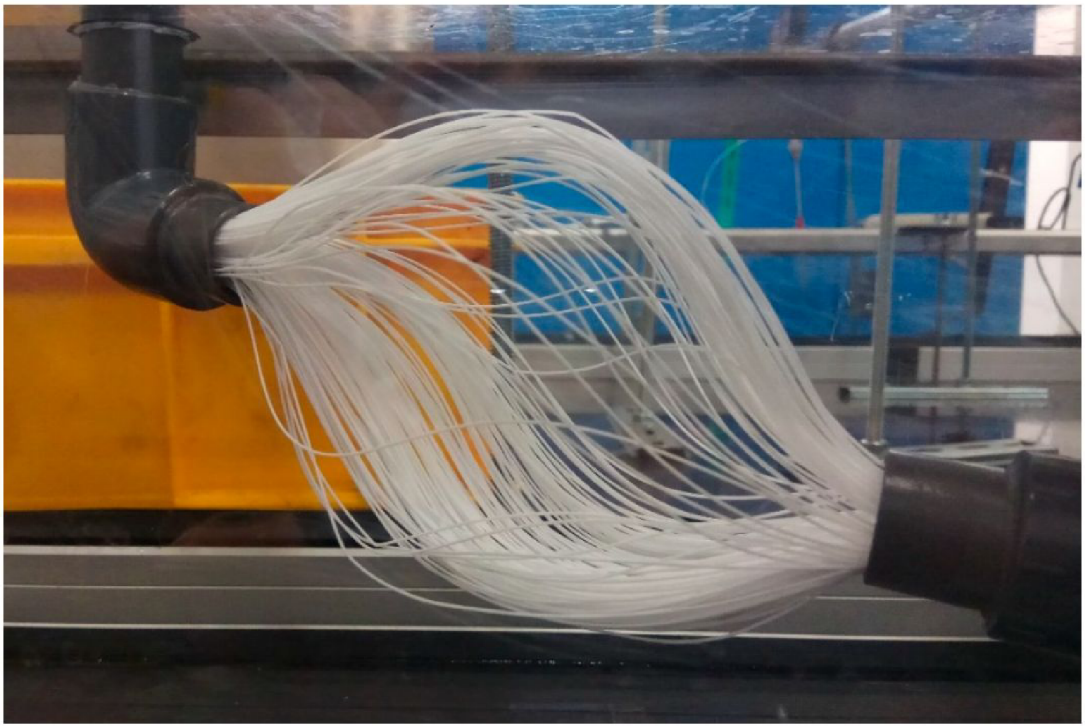

Figure B.4: Single-bundle membrane module MM002 during the experiments [5].

C Evaluated Data

Table C.1: Measured and evaluated data. Membrane input temperature, membrane mass flow rate, membrane and condenser heat transfer rates, relative thermal error, permeate flux, applied bulk inside pressure drop between input and output of the membrane, membrane and condenser thermal effectivenesses, overall heat transfer coefficient of condenser, polarization coefficient, and relative error of permeate flux prediction.

	MM002			MM003			MM004			MM006		
$u_{m,i}$ [°C]	55.11	60.02	65.24	54.68	59.97	64.55	60.33	70.09	80.06	54.32	59.13	64.43
$\dot{m}_m$ [l·h^{-1}]	270	270	270	180	480	180	65	80	65	300	300	300
q_m [W]	122	106	106	122	135	159	76	166	166	163	202	193
$-q_c$ [W]	125	113	133	129	142	167	142	193	252	167	209	209
e [%]	2.07	2.18	2.01	1.86	2.72	2.87	2.27	2.46	3.73	2.00	1.60	3.00
j [kg · m^{-2} · h^{-1}]	2.96	2.81	2.60	1.85	2.33	2.52	1.32	2.14	3.05	1.21	1.26	1.49
Δp [kPa]	100	100	100	90	120	90	30	42	30	40	40	40
η_{m} [%]	72.35	78.94	72.61	73.22	83.44	75.93	79.35	59.22	85.35	71.93	60.13	73.94
η_{he} [%]	2.85	3.38	3.49	5.23	5.46	7.50	3.88	4.53	4.87	3.34	4.30	3.99
h_c [W · m^{-2} · K^{-1}]	39.93	47.52	49.14	74.26	77.58	107.72	54.78	64.04	69.01	46.97	60.76	56.25
ψ [-]	0.46	0.40	0.38	0.47	0.46	0.48	0.27	0.35	0.32	0.55	0.59	0.53
e_p [%]	4.18	2.54	4.67	1.71	4.80	6.50	4.67	11.62	12.42	5.23	4.28	9.52

D Validation

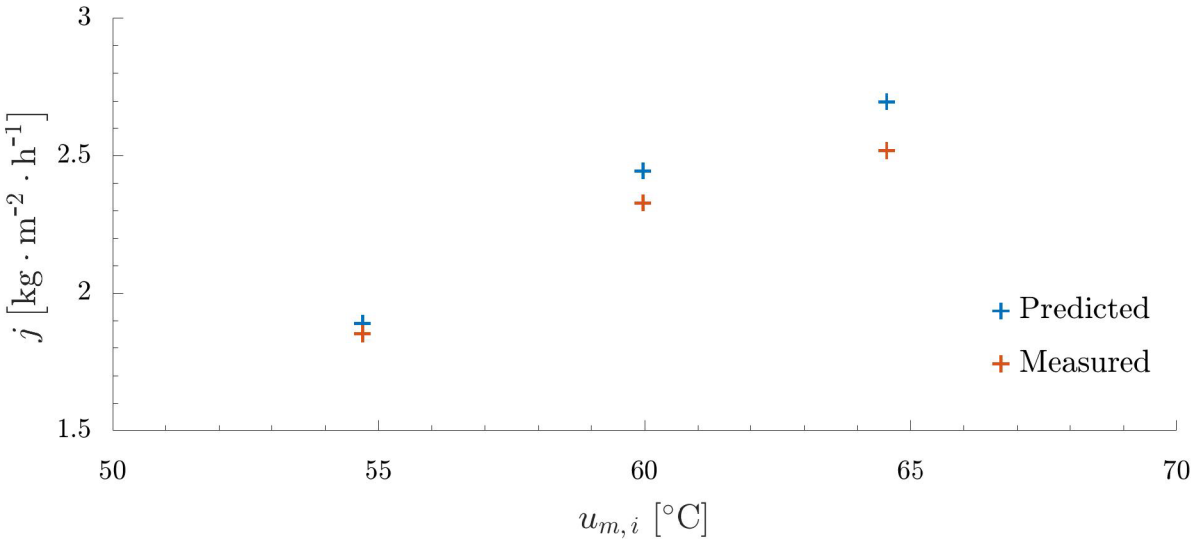

Figure D.1: Measured and predicted dependence of permeate flux on the membrane input temperature, MM003.

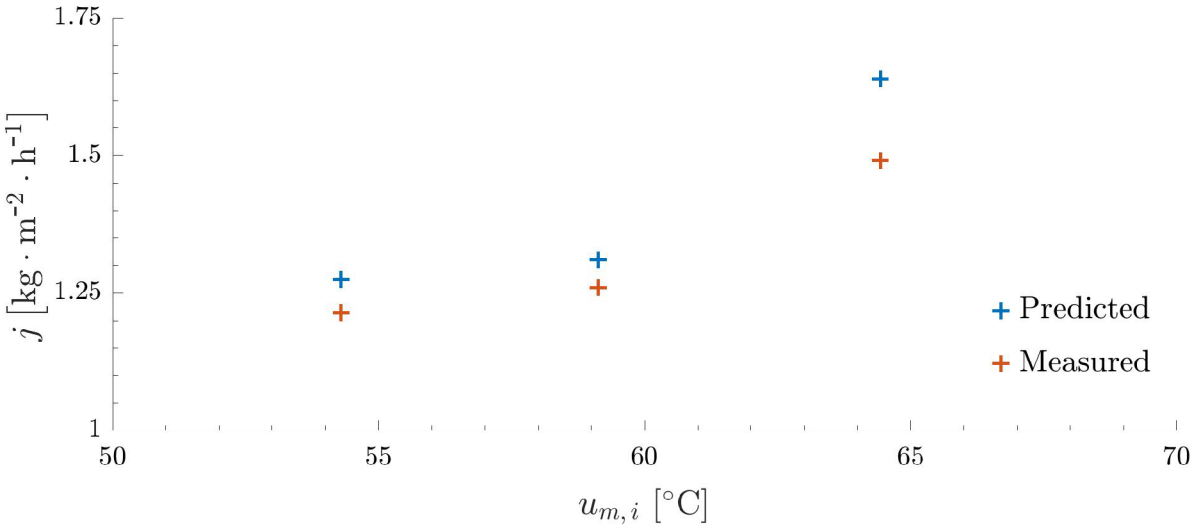

Figure D.2: Measured and predicted dependence of permeate flux on the membrane input temperature, MM006.